13

Engineering and Technology

ACTIVE FLOW CONTROL OF FLOW AROUND A CIRCULAR CYLINDER AT A SUBCRITICAL REYNOLDS NUMBER

Aritouch Puengrung[1], Maliwan Lee[2], Pongporn Preyapornmaravich[3], Thidarat Kaewkhao[4], and Kamthon Septham[5*]

Department of Mechanical Engineering, Faculty of Engineering
King Mongkut's University of Technology Thonburi, Thailand
[*]**Corresponding Author, E-mail:** kamthon.sep@kmutt.ac.th

Abstract

Several complicated flow features such as boundary-layer separation, shear layer, wake region, and vortex shedding involve in bluff-body flows causing aerodynamic drag. Active flow control is widely implemented to modify flow characteristics around a bluff body in which form drag plays an essential role due to boundary-layer separation. In the present study, the flow around a circular cylinder, a canonical flow, was investigated at Reynolds number (Re) of 3900, a sub-critical Reynolds number, to understand better the underlying physics related to drag reduction using active flow control. Synthetic jet actuators were installed at the angles of 90 and 270 degrees from the stagnation point, corresponding to the boundary-layer separation points of such flow. Synthetic jet actuators were assigned to operate at a constant frequency since the vortex shedding frequency in a sub-critical range is constant at Strouhal number (St) around 0.2. Computation fluid dynamics simulations were employed. The OpenFOAM, the open-source computational fluid dynamics software, was utilized. Unsteady Reynolds-averaged Navier–Stokes (URANS) simulations with the SST k-ω turbulence model were performed. Flows with and without synthetic jet actuators were observed. The drag coefficient (Cd) and the Strouhal number for uncontrolled flow are 0.996 and 0.207, respectively. These results agreed well with Norberg's wind tunnel experimental data (1987). For controlled flow, the drag coefficient was reduced to 0.92, equal to a 7.46% reduction. The vortex shedding frequency is also reduced to St ≈ 0.16. It is suggested that the synthetic jet actuators cause a reduction in aerodynamic drag by suppressing the occurrence of vortex shedding at the rear of a cylinder.

Keywords: Active Flow Control, Bluff-body aerodynamics, Computational fluid dynamics

Introduction

Fluid flow past objects is a phenomenon seen in daily life. When the flow past a bluff body, several flow features such as a boundary-layer separation, shear layer, wake region, and vortex shedding can be found. Flow past objects generally causes resistance in the opposite direction of fluid motion. This resistance is the so-called aerodynamic drag consisting of skin friction drag and pressure drag. Skin friction drag is related to the shear stress acting on the object's surface, while pressure drag is caused by the pressure difference between the object's front and rear ends. Considering the velocity profile of fluid flow inside the boundary layer adjacent to the surface of an object, the boundary-layer separation occurs when the velocity gradient at the wall becomes zero. This position is the separation point. In the region next to the separation point, the fluid flow separates from the surface creating the vortex shedding, shear layer, and wake region. In the wake region at the rear end of the object, the pressure is relatively low compared to the front end of the object.

Thus, the pressure drag plays a significant role in bluff-body flows. Various studies are carried out to better understand underlying physics of bluff-body flows. Flow around a circular cylinder is one of the canonical flows several researchers have investigated due to its simple geometries. Its fundamental flow physics can also be applied to complex shapes and geometries. Lienhard (1996) showed that flow past a circular cylinder can be classified into several regimes based on Reynolds number, as shown in Figure 1. In the sub-critical Reynolds number regime, $Re \approx 300$ - $3x10^5$, the transition to turbulence completely appears in the separated shear layers and the drag coefficient is invariant with Reynolds number. Panton (2013) presented the relationship between the Reynolds number and the drag coefficient of the flow past the circular cylinder as shown in Figure 2. The drag coefficient in the sub-critical Reynolds number regime is rather constant.

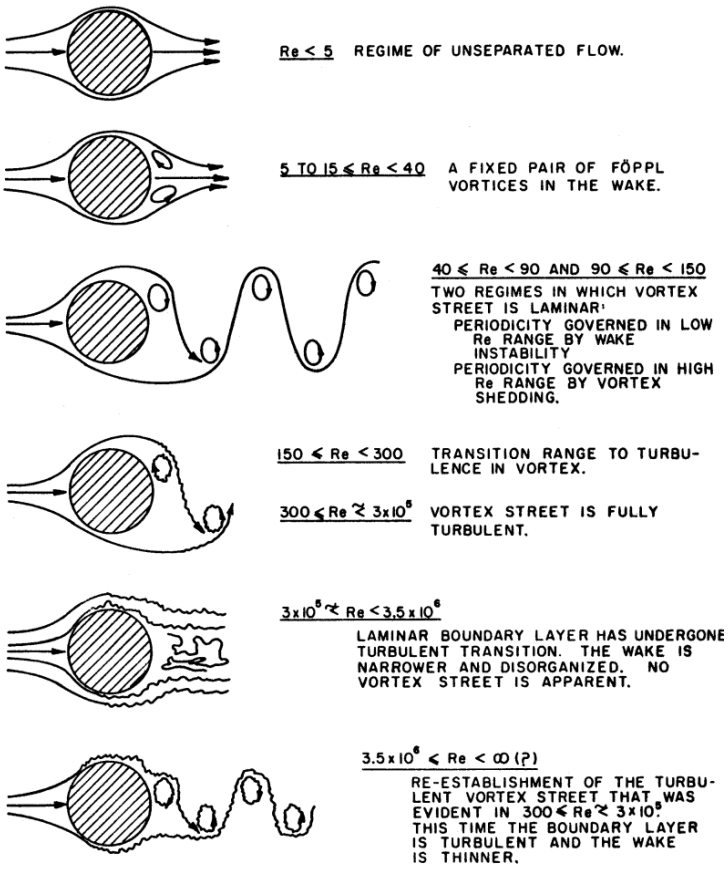

Figure 1: Regimes of flow past a circular cylinder

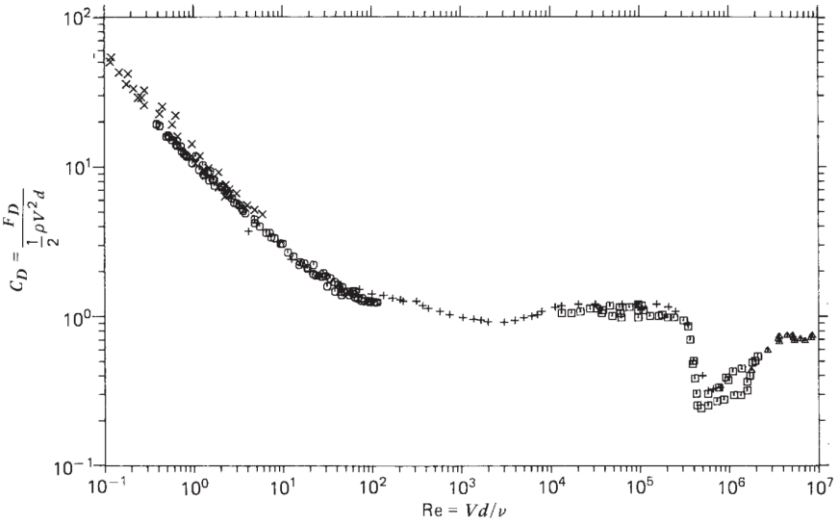

Figure 2: The drag coefficient versus Reynolds number of flow past a circular cylinder

Several flow control techniques have been implemented to reduce the aerodynamic drag of a bluff body. In general, it can classify into two methods: passive flow control and active flow control. No external energy source is needed for passive flow control, such as modifying the object's shapes and geometries. For active flow control, energy input is required to activate the controlled devices, such as the synthetic jet actuators and moving surfaces.

The study of flow past a circular cylinder at Reynolds number = 3900 using large eddy simulation (LES) reveals that the separation point occurs at the angles of approximately 90 and 270 degrees measured from the stagnation point (Rajani, 2015). Moreover, the Strouhal number and the drag coefficient are rather constant in the sub-critical Reynolds number regime. Thus, it is interesting to explore the underlying physics related to drag reduction of flow around a circular cylinder at *Re* = 3900 using active flow control.

Computation fluid dynamics simulations were employed. The OpenFOAM, the open-source computational fluid dynamics software, was utilized. Unsteady Reynolds-averaged Navier–Stokes (URANS) simulations with the SST k-ω turbulence model were performed. Flows with and without synthetic jet actuators were observed.

Research Objective (s)

1. To investigate the underlying physics of flow around a circular cylinder at Reynolds number equal to 3900 with and without synthetic jet actuators.
2. To study the influence of active flow control on drag reduction of the flow around a circular cylinder at Reynolds number equal to 3900 using synthetic jet actuators at 90 and 270 degrees.

Literature Review

Typically, seven main distinct flow regimes occur in the flow past a circular cylinder over a vast range of Reynolds numbers (Lienhard, 1996). The initial regime demonstrated a steady and unsteady flow at *Re* lower than 5. In the second regime, the pair of vortices appear in the wake region when *Re* is between 5 and 40. The wake region in the regime of *Re* between 40 and 90 becomes unstable. In the following range of Reynolds number, laminar vortex shedding occurs between *Re* =

90 and 150. At *Re* = 150 to 300, the separated shear layers become turbulent. The vortex street becomes turbulent between *Re* = 300 and $3x10^5$ in the following regime. No vortex street appears between *Re* = $3x10^5$ and $3.5x10^6$. The wake region is relatively thin, and the boundary layer changes into turbulence. The vortex street is re-established, and the boundary layer is turbulent at *Re* greater than $3.5x10^6$. Liu (2018) demonstrated that the results obtained from large eddy simulations of flow around a circular cylinder at *Re* = 3900 agreed well with Norberg's wind tunnel experimental results (1987).Various techniques of flow control have been applied to flow past objects. For passive flow control, the splitter plate was installed behind the circular cylinder to suppress the vortex-shedding mechanisms (Buresti, 1998). For active flow control, synthetic jet actuators were utilized to reduce the aerodynamic drag of flow around a circular cylinder (Gad-el-Hak, 2003). Implementing the dielectric barrier discharge (DBD), plasma actuator reduced the aerodynamic drag of flow around a circular cylinder by 14% (Akbiyik et al., 2018). Zhang and Samtaney (2015) performed numerical simulations of the airfoil with synthetic jets. The domain of synthetic jets was defined as an airfoil surface discontinuity instead of being of the cavity-type synthetic jets. The velocity profile of the jet slot was set to be the Poiseuille-type with a sinusoidal function. In sub-critical Reynolds numbers, synthetic jet actuators were applied to flow past the circular cylinder at *Re* = 3900. Catalano et al. (2002) applied synthetic jet actuators with a momentum coefficient (C_μ) of 6.5×10^{-3} and a dimensionless frequency (f^+) = 9.2. The synthetic jet actuators were located at a circular cylinder angle of 85.12°. The results show that the drag coefficient was decreased by 13%. Fujisawa and Takeda (2003) performed numerical simulations of flow past a circular cylinder at *Re* = 9000 with synthetic jet actuators. The momentum coefficient was assigned at 3.6×10^{-3}, and the dimensionless frequency was varied between 1 and 5. The synthetic jet actuators were located at 90. It demonstrated that the optimum drag reduction was 30% at $f^+ = 4$.

Methodology

There are four steps in the methodology of this work; the first step is to specify the computational domain, the second step is to specify the parameters and condition of the fluid, the third step is the fluid domain's mesh generating, the final step is run the simulation in OpenFOAM and collect the results data.

Part 1: Define the computational domain.

The computational domain was adopted from Liu (2018), as shown in Figure 3. The diameter of the cylinder was D. The streamwise length from the inlet to the cylinder was 10D, and the distance from the cylinder to the outlet was 25D. The wall-normal distance from the wall to the cylinder was 8D. The spanwise length is πD, where D was 10 cm.

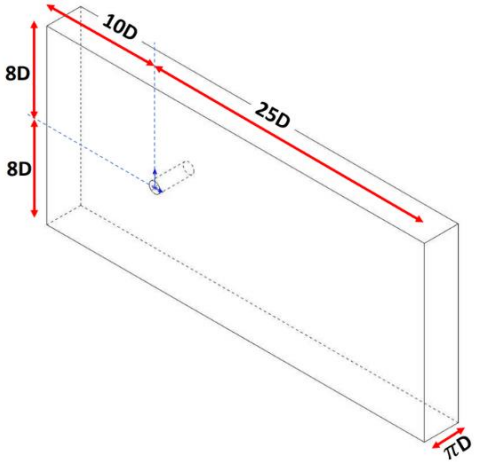

Figure 3: Geometry.

Part 2: Specify the boundary conditions.

The boundary conditions are presented in Figure 4 and summarized in Table 1. The boundary condition for the inlet was the free-stream velocity U_∞ = 1 m/s with zero pressure gradients. The outlet pressure was specified as 0 Pa. At the top and bottom walls, the free-slip boundary condition was assigned. The cylinder surface was defined as the no-slip wall. The symmetry plane was set for the front and back of the domain. The fluid flow was incompressible flow at Re = 3900.

Table 1: Boundary condition of flow past around a circular cylinder

Location	Boundary condition
Inlet	Free-stream velocity, U_∞ =1 m/s
Outlet	Static pressure 0 Pa
Top and bottom	Free slip wall
Front and back	Symmetry
Cylinder	No slip wall

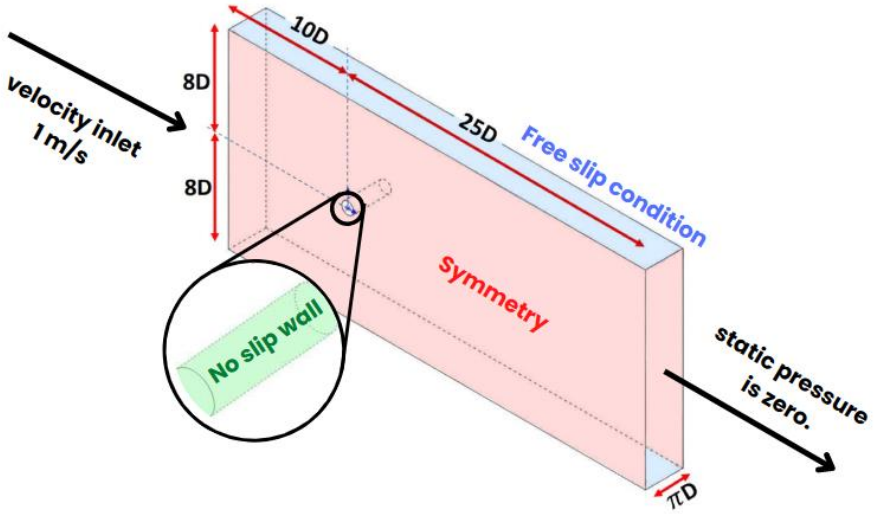

Figure 4: Boundary condition

Part 3: Fluid domain's mesh generating.

The meshes were generated by dividing the fluid domain into several elements. In the present study, the "Multizone" type was utilized. The type of mesh was hexahedral, as presented in Figure 5.

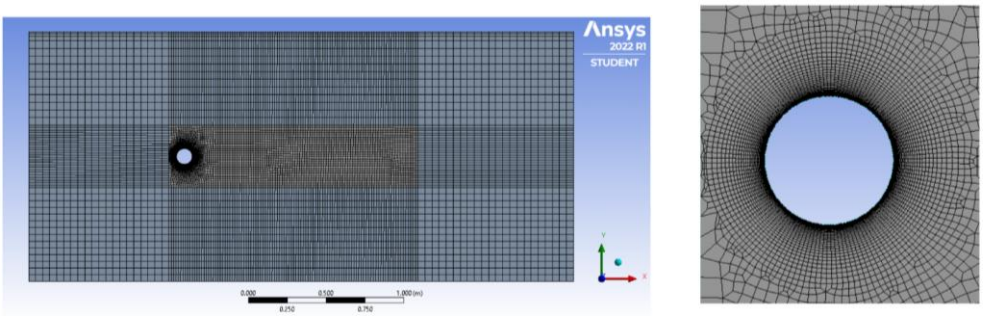

Figure 5: Meshing

Moreover, the near-wall model was implemented. It suggests that, in the viscous sub-layer, it is necessary to achieve y+ <1 for the first cell adjacent to the cylinder surface. The quadratic mesh applies to the near-wall domain, and the inflation layers around the surface of the cylinder were added. As a result, the maximum y+ around the cylinder was approximately 0.5. It noted that 35 inflation layers were used.

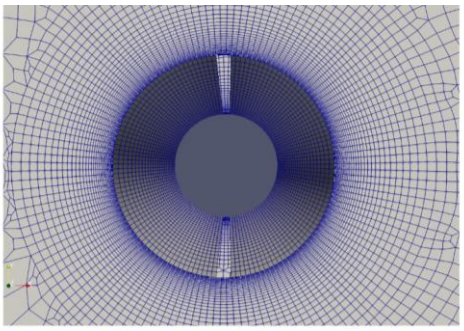

Figure 6: The location of synthetic jets

The synthetic jet actuators were located at 90 and 270 degrees. The width of the slot was 0.005 m. The spanwise length was πD, in which D was 10 cm.

Part 4: Run the simulations and collect the results data.

Numerical techniques based on the incompressible Navier-Stokes equation were used to examine the physical phenomena of the flow around a circular cylinder using computational fluid dynamics (CFD). The unstable Reynolds-averaged Navier-Stokes (URANS) equation was used in the current investigation. Equations (1) and (2) present the momentum and continuity equations.

$$\frac{D\bar{u}_i}{Dt} = \frac{\partial \bar{p}}{\partial x_j} + \nu \frac{\partial^2 \bar{u}_i}{\partial x_j \partial x_j} - \frac{\partial \tau_{ij}}{\partial x_j} \quad (1)$$

$$\frac{\partial \bar{u}_i}{\partial x_i} = 0 \quad (2)$$

where τ_{ij} denotes the nonlinear Reynolds stress terms. Thus, the Boussinesq hypothesis is used to solve the URANS equation by redefining the Reynolds stress terms in equation (3) as follows:

$$\tau_{ij} = -\rho\overline{u'v'} = \mu_t\left(\frac{\partial \bar{u}_j}{\partial x_i} + \frac{\partial \bar{u}_i}{\partial x_j}\right) \tag{3}$$

The k-ω SST turbulence model models the kinematic eddy viscosity. The transport equations, turbulent kinetic energy, and specific dissipation equations are presented in equations (4) and (5), respectively.

$$\frac{\partial k}{\partial t} + U_j\frac{\partial k}{\partial x_j} = P_k - \beta^* k\omega + \frac{\partial}{\partial x_j}\left[(v + \sigma_k v_T)\frac{\partial k}{\partial x_j}\right] \tag{4}$$

$$\frac{\partial \omega}{\partial t} + U_j\frac{\partial \omega}{\partial x_j} = \alpha\omega^2 - \beta\omega^2 + \frac{\partial}{\partial x_j}\left[(v + \sigma_\omega v_T)\frac{\partial \omega}{\partial x_j}\right] + 2(1 - F_1)\sigma_{\omega_2}\frac{1}{\omega}\frac{\partial k}{\partial x_i}\frac{\partial \omega}{\partial x_i} \tag{5}$$

Results

Flow past a circular cylinder without a synthetic jet

Considering the flow past a circular cylinder without a synthetic jet, the graph of the relation between drag coefficient and time is shown in Figure 7. During the transient period, the first ten seconds, the drag coefficient dramatically fluctuated. The value of the drag coefficient is constant after the vortex shedding has repeatedly occurred, and the average drag coefficient is 0.996. As compared result from Norberg (1987), Reynolds number 3900 is 0.98 and has a tolerance of 0.05 as presented in Table 2.

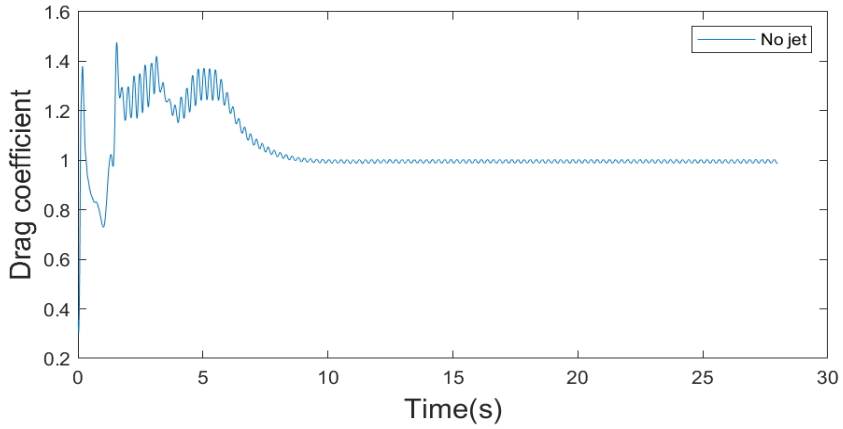

Figure 7: The relation between drag coefficient and time

The graph of the relationship between frequency and amplitude is shown in Figure 8. The vortex shedding occurred at 2.07 Hz. As a result, the Strouhal number is 0.207, and Norberg (1987) is 0.215. The obtained values from the simulation and experiment are close to each other.

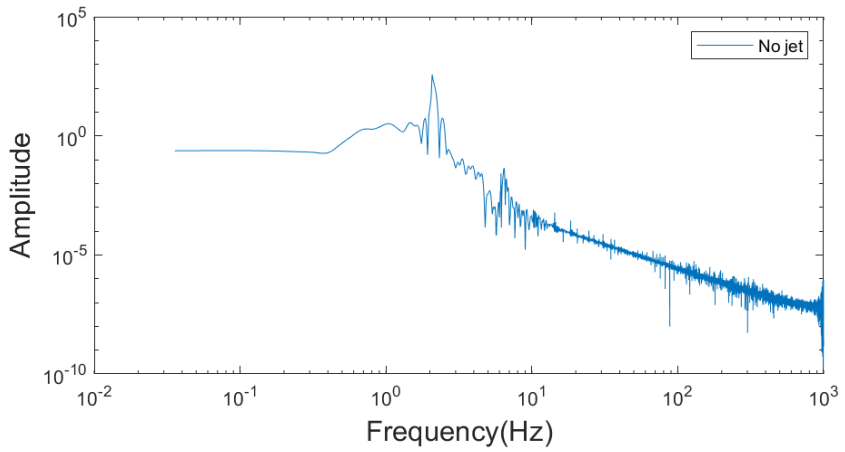

Figure 8: The relation between frequency and amplitude

Flow past a circular cylinder with synthetic jets at 90 and 270 degrees.

When comparing the drag coefficients before and after jet injection, the drag coefficient from jet injection is less than without jet injection. The simulation result of no jet and attached jet is shown in Figure 9. By attaching the synthetic jet at 90 and 270 degrees which starts actuated at 10.6 seconds, the average drag coefficient after the vortex shedding occurs was 0.92. It can conclude that using synthetic jets could reduce the drag coefficient by 7.46%.

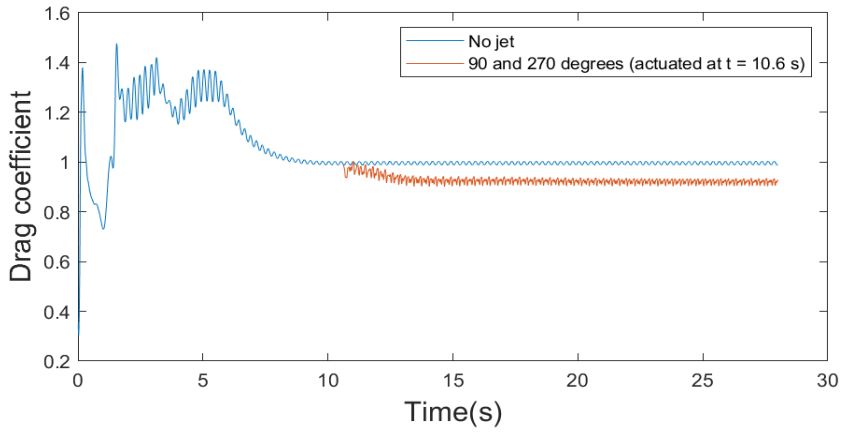

Figure 9: The simulation result of drag coefficient of no jet and attached jet

Comparing flow past a circular cylinder with and without jet

Figure 10 presents the power spectral density of the lift coefficient of flow around a circular cylinder with and without synthetic jet actuators. For uncontrolled flow, one peak was detected at frequency around 2.07 Hz, corresponding to the vortex shedding frequency. For controlled flow, two peaks were detected at frequencies of 1.61 and 8.22 Hz, corresponding to the vortex shedding frequency and the oscillation frequency of synthetic jet actuators, respectively.

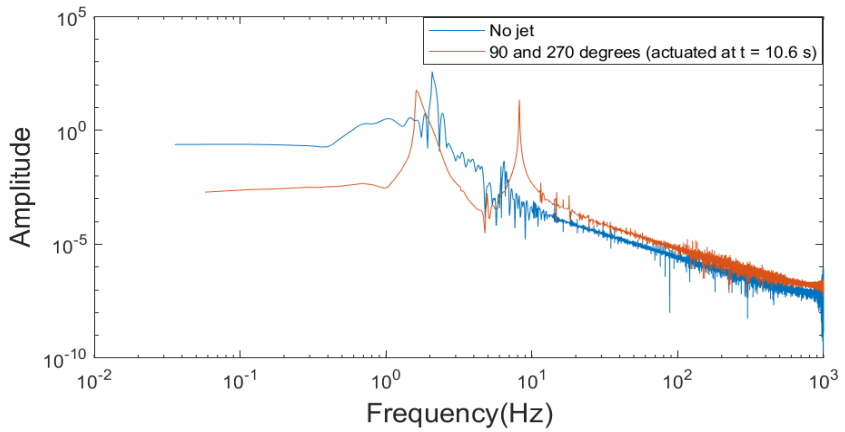

Figure 10: The relationships between amplitude and frequency of simulation result

Table 2: The comparison of the mean drag coefficients and Strouhal number between 2 cases

Case	C_D	St
Norberg, C. (1987)	0.98±0.05	0.215±0.005
Uncontrol	0.996	0.207
Control	0.92	0.161
Percentage different	7.46%	

Comparing the streamwise velocity contour

A comparison of the streamwise velocity contour between non-jet and synthetic jets cases found that installing synthetic jets will reduce the frequency of vortex generated at the back of the cylinder. It decreases vortex strength and drag coefficient.

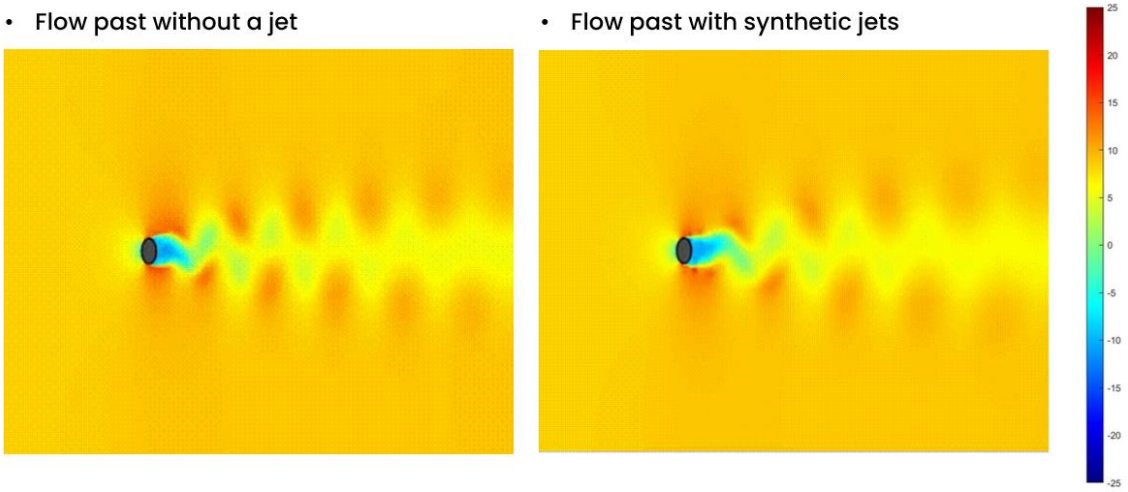

Figure 11: The streamwise velocity contour between non-jet and synthetic jets

Discussion

From Figure 7, it is observed that the drag coefficient before vortex shedding fluctuates. After that, the drag coefficient is constant. The simulation results show that the flow range at the subcritical Reynolds number 3900, the drag coefficient is 0.996. The comparison of the drag coefficient between the simulation and the Norberg experiment has a deviation of 1.63 percent. Figure 8 shows that the

Strouhal flow frequency around a circular cylinder is 2.072 Hz. The calculated Strouhal number is 0.207, and compared with the results of Norberg, there is a difference of 3.72%. Results obtained from OpenFOAM simulation are close to experimental results in the part of drag coefficient and Strouhal number. Therefore, the synthetic jets are installed as shown in the 3D circular cylinder model at angles of 90 and 270 degrees, and the results are shown in Figures 9 and 10. Figure 9 shows the drag coefficient after 10.6 seconds when installing synthetic jets is reduced. The average drag coefficient is 0.92, indicating a 7.46% reduction in drag compared to a circular cylinder without synthetic jets. In Figure 10, the Strouhal frequency from attaching synthetic jets will decrease and equal 1.61 Hz. It also causes another peak at Jet frequency, which is 8.224 Hz. As a result, the installation of synthetic jets affects the flow characteristics. Figure 11 shows the streamwise velocity contour of the case with synthetic jets, and the frequency generated by the vortex at the back of the circular cylinder is lower than without synthetic jets.

Conclusion

For the study of flow around a circular cylinder at a subcritical Reynolds number (Re=3900), OpenFOAM software is used for simulation, and Unsteady Reynolds-averaged Navier-Stokes (URANS) equations with the k-ω SST turbulence model are employed. From the simulation result, it is observed that OpenFOAM software is a program that provides accurate results. Compared with experimental results, the drag coefficient has a tolerance of 1.63%. For the Strouhal number, there is an error of approximately 3.72%. Moreover, installing synthetic jets at 90 and 270 degrees angles can reduce the drag coefficient by 7.46%. Comparing the streamwise velocity contour, installing synthetic jets will reduce the vortex frequency at the back of the circular cylinder.

References

Akbıyık, H., Akansu, Y. E., & Yavuz, H. (2017). Active control of flow around a circular cylinder by using intermittent DBD plasma actuators. *Flow Measurement and Instrumentation*, *53*, 215-220.

Buresti, G. (1998). Vortex shedding from bluff bodies. *Wind effects on buildings and structures*, 61-95.

Catalano, P., Wang, M., Iaccarino, G., & Sbalzarini, I. F. (2002). Optimization of cylinder flow control via actuators with zero net mass flux. In *Proceedings of the Summer Program* (p. 297). Stanford, CA, USA: Center for Turbulence Research.

Fujisawa, N., & Takeda, G. (2003). Flow control around a circular cylinder by internal acoustic excitation. *Journal of Fluids and Structures*, *17*(7), 903-913.

Gad-el-Hak, M., Pollard, A., & Bonnet, J. P. (Eds.). (2003). *Flow control: fundamentals and practices* (Vol. 53). Springer Science & Business Media.

Lienhard, J. H. (1966). *Synopsis of lift, drag, and vortex frequency data for rigid circular cylinders* (Vol. 300). Pullman, WA: Technical Extension Service, Washington State University.

Liu, H. (2018, July). Large eddy simulation of flow past a 3D cylinder at Re= 3900. In *IOP Conference Series: Materials Science and Engineering* (Vol. 383, No. 1, p. 012050). IOP Publishing.

Norberg, C. (1987). Effects of Reynolds number and a low-intensity freestream turbulence on theflow around a circular cylinder. *Chalmers University, Goteborg, Sweden, Technological Publications*, *87*(2), 1-55.

Panton, R. L. (2013). *Incompressible flow*. John Wiley & Sons.

Zhang, W., & Samtaney, R. (2015). A direct numerical simulation investigation of the synthetic jet frequency effects on separation control of low-Re flow past an airfoil. *Physics of Fluids*, *27*(5), 055101.

DECENTRALIZED CRYPTOCURRENCY EXCHANGE PLATFORM FOR VERY SMALL POWER PLANT (VSPP)

Weerawut Thanhikam

Faculty of Engineering and Technology
Panyapiwat Institute of Management
Corresponding Author, E-mail: weerawuttha@pim.ac.th

Abstract

This research explores the integration of decentralized cryptocurrency exchange platforms with Very Small Power Plants (VSPPs) to enhance energy trading efficiency and security. The study investigates the history and applications of digital currencies, as well as the evolution of energy trading from centralized systems to VSPPs. By examining the technical requirements and challenges of integrating decentralized exchange platforms with VSPP systems, the research aims to provide insights into the potential benefits and obstacles of this integration. The objective is to contribute to the development of sustainable energy systems by leveraging decentralized technologies for more efficient and secure energy trading.

The research findings demonstrate the effectiveness of the energy trading system developed in this study. The system showcases a low transaction error rate of approximately 6.481% out of 324 transactions, highlighting its reliability. Additionally, the system offers cost efficiency with a gas fee of less than 0.0001 NEAR per transaction (equivalent to less than $0.01 or 0.34 THB), outperforming other platforms that average around $3.79 (130.57 THB) and $0.68 (23.43 THB) per transaction. These results underscore the system's reliability, low error rate, and cost-effectiveness in facilitating efficient energy trading.

Keywords: Decentralized Finance, Automated Market Maker, Cryptocurrency, Energy Trading, Blockchain, Smart Contract

Introduction

The world's increasing energy demand has sparked interest in decentralized energy systems, such as Very Small Power Plants (VSPPs), which generate electricity from renewable sources. However, efficient and secure energy trading remains a challenge for VSPPs. To address this, we propose integrating a Decentralized Cryptocurrency Exchange Platform with VSPPs, leveraging blockchain technology for security and efficiency. This integration offers benefits such as enhanced energy trading, reduced transaction costs, increased market transparency, and promotion of renewable energy sources. By revolutionizing energy generation and trading, this integration can accelerate the transition to a sustainable and decentralized energy system.

According to Capponi and Jia (2021), the adoption of blockchain-based decentralized exchanges has gained significant attention in recent years. Blockchain technology, described as a decentralized database managed by multiple participants, has significantly transformed the financial industry, enabling the implementation of self-executing and intermediary-free smart contracts (Zetzsche et al., 2020; Yaga et

al., 2019). Smart contracts offer a range of advantages such as enhanced security, transparency, efficiency, and cost savings across various sectors, including finance, real estate, healthcare, and supply chain management (Xu et al., 2021; Han et al., 2021; Qin et al., 2021). By eliminating the need for trust and automating complex transactions, smart contracts have the potential to revolutionize industries, fostering the development of secure, efficient, and transparent systems (Di Pierro, 2017; Malumad & Rostek, 2017; Delgado-Segura et al., 2018).

Eventually, the integration of a Decentralized Cryptocurrency Exchange Platform with VSPPs offers a solution to the challenges of efficient and secure energy trading. This technology harnesses the power of blockchain and smart contracts to revolutionize energy systems and promote sustainability.

This manuscript is organized as follows. The introduction provides a brief overview of blockchain and VSPP, establishing the foundation for the research. The next section introduces the research objectives, followed by a comprehensive literature review related to the topic. The methodology section outlines the approach and methods used in the study. The subsequent section presents the findings and discussions based on the research results. Finally, the conclusion summarizes the key insights and contributions of the study.

Research Objective (s)

The research objective of this study is to examine and evaluate the adoption and performance of blockchain-based decentralized exchanges (DEX) in the context of energy trading. Specifically, the study aims to analyze transaction errors and gas fees associated with DEX platforms, comparing them with centralized exchanges. The research seeks to provide insights into the efficiency, reliability, and cost-effectiveness of DEX in facilitating energy trading and assess their potential for revolutionizing the current financial landscape.

Literature Review

The technology known as Blockchain originated from Satoshi Nakamoto's research paper titled "Bitcoin: A Peer-to-Peer Electronic Cash System" (Nakamoto, 2008), which served as the initial introduction of Blockchain and Bitcoin. Although this seminal work is considered groundbreaking, it was not published in a peer-reviewed journal, and the identity of the author remains anonymous. The impact of Blockchain extends beyond cryptocurrency and has led to significant transformations in the financial industry and beyond (Farell, 2015; Delgado-Segura et al., 2018).

In the context of decentralized cryptocurrency exchanges, a study by Han, Huang, and Zhong (2021) examined how investors make price-related decisions when comparing Uniswap, a decentralized exchange, with Binance, a centralized exchange. Their research demonstrated that the provision of liquidity pools facilitates investors' transition from Binance to utilizing Uniswap, indicating that Uniswap has gained investor trust and achieved value proposition in the cryptocurrency realm.

Malumad and Rostek (2017) developed an equilibrium model for a decentralized cryptocurrency exchange (Dex) and highlighted the advantages of Dex in managing certain risks that cannot be achieved in a centralized exchange (Cex). Despite the risks associated with price impact, investors continue to engage with decentralized exchanges.

Furthermore, the study by Capponi and Jia (2021) sheds light on the essential workings of liquidity pooling in automated market makers (AMMs) within decentralized cryptocurrency exchanges. It emphasizes factors beyond high transaction fees and explores the nature of liquidity pooling.

These references provide insights into the concepts and dynamics of blockchain technology, decentralized exchanges, and the potential of smart contracts in revolutionizing various industries.

Methodology

The methodology for developing the decentralized cryptocurrency exchange platform, which facilitates peer-to-peer digital currency exchange without a central authority using blockchain technology, involves two user types: traders and liquidity providers. To enable exchange transactions, liquidity providers are essential. Referring to Picture 1, Exchange Overview, when a liquidity provider deposits 10 coins of Token A and 1 coin of Token B, they are then calculated and receive 4 LP shares in return. The deposited coin pair goes into the reserve pool. Traders who come to exchange will do so from this pool, and liquidity providers receive rewards through yield farming, derived from transaction fees imposed on traders.

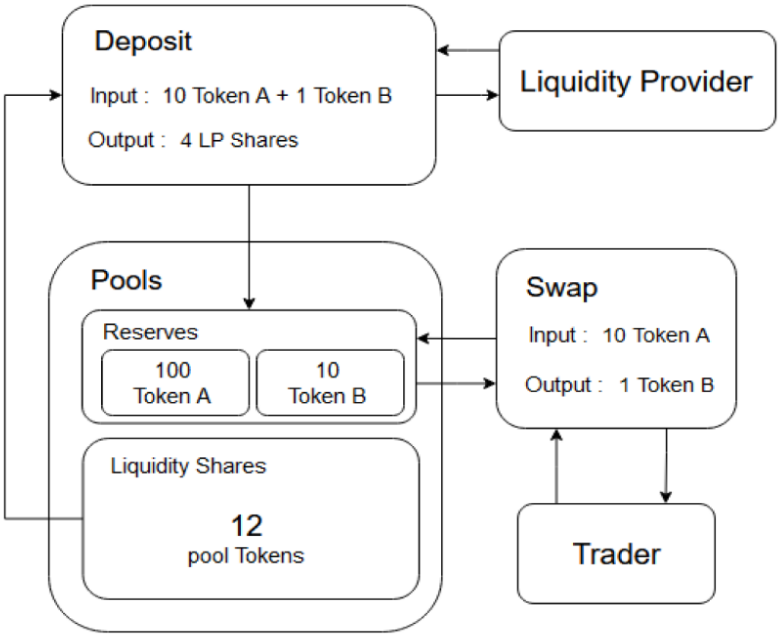

Picture 1: Exchange Overview

In the exchange process, referring to Picture 2 (Exchange Rate Calculation), if a trader wants to exchange 3 coins of Token A for 1 coin of Token B, they would need to pay 3 Token A coins plus a 1% transaction fee. As a result, they would receive 1 coin of Token B in return. After the exchange, the exchange rate would be recalculated, and the price would adjust to approximately 1 Token B equal to ~3.015 Token A, according to the equation $X \times Y = K$, where the price fluctuates along this curve based on the mechanics of a free market (Jiahua Xu, Krzysztof Paruch, Simon Cousaert, Yebo Feng, 2021)

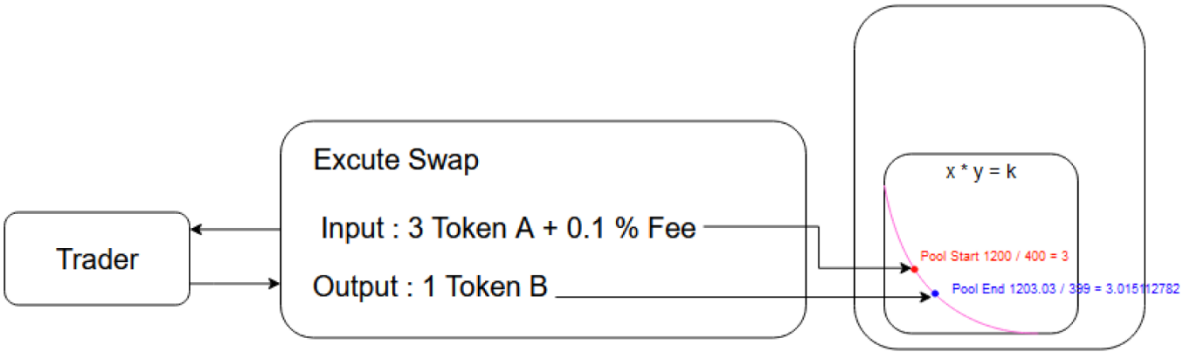

Picture 2: Exchange Rate Calculation

In terms of the exchange process, for a VPP (Virtual Power Plant) acting as an energy trader who wishes to exchange 3 units of Energy Token A for 1 unit of Energy Token B, they would need to pay 3 units of Energy Token A plus a 1% transaction fee. After the exchange, they would receive 1 unit of Energy Token B in return. Once the exchange is completed, the exchange rate would be recalculated, resulting in 1 unit of Energy Token B being equivalent to approximately 3.015 units of Energy Token A, following the curve equation $X \times Y = K$. The price would fluctuate along this curve based on the mechanisms of a free market.

List of the tools used in this research are following

React JavaScript library: This tool is utilized to facilitate the development of the website in a convenient and highly efficient manner. React is a popular JavaScript library that allows for the creation of interactive user interfaces, making web development more streamlined and responsive.

Rust: Rust is a programming language used for developing smart contracts on the NEAR Protocol using the near-sdk-rs. It provides a secure and efficient environment for writing and executing smart contracts, ensuring the reliability and integrity of the decentralized exchange platform.

NEAR testnet: The NEAR testnet serves as a blockchain server specifically designed for testing websites built on the NEAR Protocol. It provides a sandboxed environment where developers can test and validate their applications before deploying them on the mainnet, ensuring smooth functionality and identifying any potential issues or bugs.

near-api-js: This is a NEAR library that assists in accessing various services offered by NEAR and facilitates communication with smart contracts. It provides developers with a set of tools and functionalities to interact with the NEAR blockchain, making it easier to integrate and utilize the features and capabilities of the decentralized exchange platform.

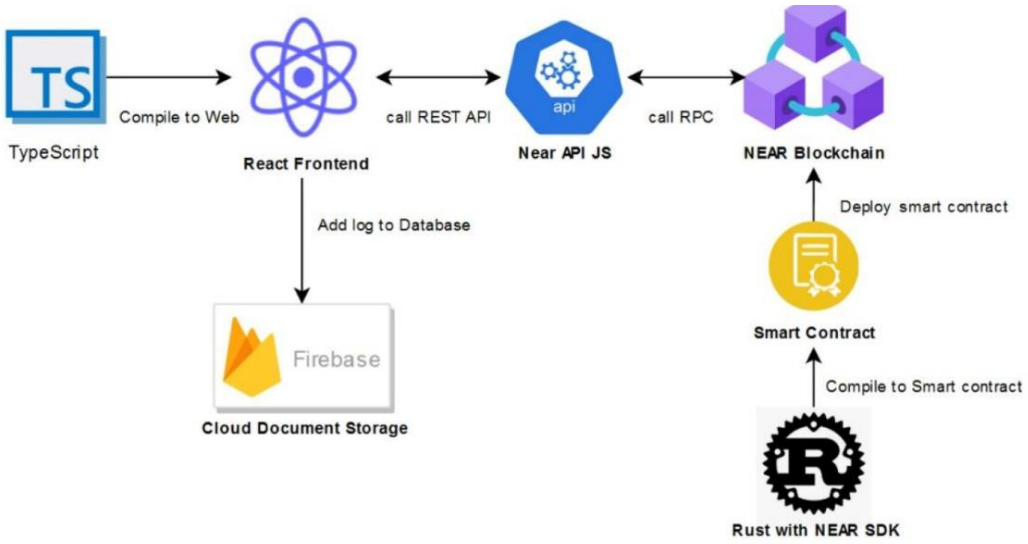

Picture 3: Structure of the Exchange System

The React frontend, as depicted in Picture 3, establishes a connection with the blockchain through NEAR API JS. The smart contract, which is compiled from Rust, is integrated into the system using NEAR API JS. The React frontend serves as the user interface, allowing users to interact with the decentralized exchange platform.

Additionally, the frontend system stores data in Firebase. This implies that the system utilizes Firebase as a data storage solution, where relevant information and user data can be securely stored. This data can then be utilized for research analysis and measuring the outcomes of the study.

In summary, the system architecture involves the React frontend connecting to the blockchain through NEAR API JS, utilizing a smart contract compiled from Rust. The frontend system further incorporates Firebase as a means of storing data for research purposes.

Results

To analyzing the result, this research evaluate the performance and feasibility of the developed decentralized exchange platform from mainly two factors, Transaction error and Gas fee. Lower transaction errors and reduced gas fees indicate improved user experience and cost-efficiency, which are essential factors for the success of such platforms.

Transaction error: This metric measures the proportion of unsuccessful transactions out of the total number of transactions. It provides insights into the reliability and efficiency of the decentralized exchange platform. A lower transaction error rate indicates a more stable and robust system.

Gas fee: Gas fee refers to the cost of executing operations on the blockchain. In comparison to other decentralized exchanges (Dex), the gas fee in this research is observed to be lower. This suggests that the developed platform offers a cost-effective solution for users, reducing the expenses associated with transaction fees.

Picture 4: User Interface of the Exchange System

The user interface (UI) displayed in Picture 4 serves as the basis for evaluating the research results. This UI presents a user-friendly interface for exchanging digital currencies. It features an input field where users can enter the desired amount of currency for the exchange, along with a button that directs them to the page where they can select the specific coins they wish to exchange.

The page for selecting the energy tokens to exchange consists of a search field for finding the desired energy currency. The page for displaying the available energy token pairs for deposit and earning rewards allows users to toggle between viewing all token pairs or the ones they have already deposited as an energy trader. On the page for entering the desired amount of energy token pairs to deposit at a consistent ratio, the available quantity of tokens is displayed. If the quantity is insufficient, the deposit cannot be made. The page for displaying the details of the deposited energy token pair shows the energy trader's share in the energy pool as a proportion and the accrued profits. Users can also click a button to initiate a withdrawal of their energy tokens.

The research results reveal valuable insights regarding our energy trading system. First, in terms of transaction error, out of a total of 324 transactions, only 21 were found to be unsuccessful, accounting for a relatively low error rate of approximately 6.481%. This indicates the robustness and reliability of our system in facilitating smooth and successful transactions.

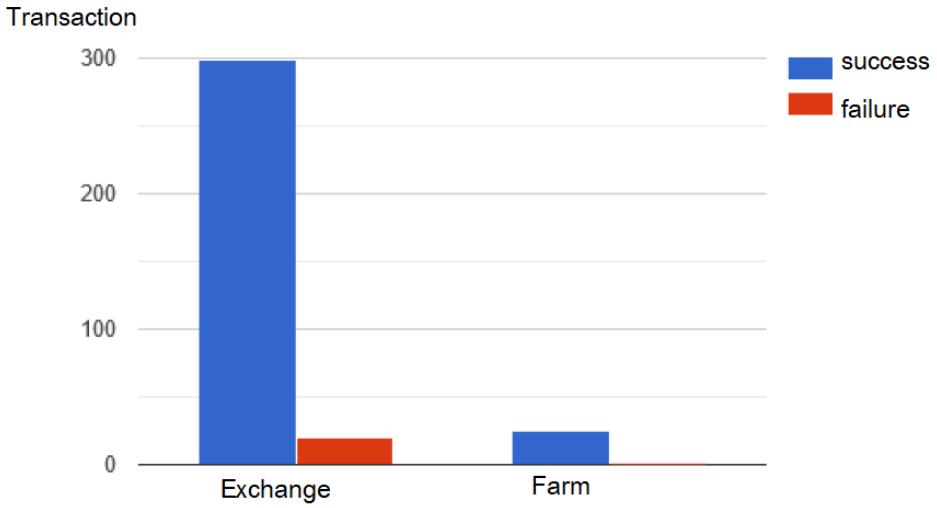

Picture 5: Performance of the Exchange System

Furthermore, when considering the gas fee, our system proves to be highly cost-effective. With a gas fee of less than 0.0001 NEAR per transaction, which is equivalent to less than $0.01 (0.34 THB), our platform offers significantly lower transaction costs compared to other prominent platforms. For instance, UniSwap averages around $3.79 (130.57 THB), while Pancake Swap stands at around $0.68(23.43 THB) per transaction. This demonstrates the competitive advantage of our energy trading system in terms of cost efficiency.

Discussion

These research findings affirm the effectiveness and efficiency of our developed system. With a low transaction error rate and minimal gas fees, our platform provides users with a seamless and cost-effective experience in energy trading. The results validate the successful integration of React JavaScript library, Rust programming language for Smart Contract development, NEAR testnet as the blockchain server, and near-api-js library for interacting with smart contracts.

Conclusion

In conclusion, our research showcases a promising energy trading system that leverages cutting-edge tools and technologies. The low transaction error rate highlights the reliability of the platform, while the minimal gas fees contribute to its cost-effectiveness. Moving forward, these research outcomes lay a solid foundation for further advancements and potential real-world applications of our energy trading system in revolutionizing the digital currency exchange landscape.

References

Buterin, V. (2017). *A next-generation smart contract and decentralized*. https://ethereum.org/en/whitepaper/

Capponi, A., & Jia, R. (2021). The Adoption of Blockchain-based Decentralized Exchanges.

Delgado-Segura, S., Pérez-Solà, C., Herrera-Joancomartí, J., Navarro-Arribas, G., & Borrell, J. (2018). Cryptocurrency Networks: A New P2P Paradigm. Mobile Information Systems.

Di Pierro, M. (2017). What Is the Blockchain?. *Computing in Science & Engineering*, *19*(5), 92-95.

Farell, R. (2015). An Analysis of the Cryptocurrency Industry.

Gackenheimer, C., & Paul, A. (2015). *Introduction to React (Vol. 52). Apress.Adams, H., Zinsmeister, N., & Robinson, D. (March 2020). Uniswap v2 Core*. https://uniswap.org/whitepaper.pdf

Han, J., Huang, S., & Zhong, Z. (2021). An Empirical Study of the Decentralized Exchange.

Malumad, S., & Rostek, M. (2017). Decentralized Exchange. American *Economic Review, 107*(11), 3320-3362.

Matsakis, N. D., & Klock, F. S. (December 2014). The Rust Language. *ACM SIGAda Ada Letters, 34*(3), 103-104.

Nakamoto, S. (2008). *Bitcoin: A Peer-to-Peer Electronic Cash System*. https://bitcoin.org/bitcoin.pdf

NEAR Foundation. (2021). *The NEAR White Paper*. https://near.org/papers/the-official-near-white-paper/

Qin, K., Zhou, L., Afonin, Y., Lazzaretti, L., & Gervais, A. (2021). CeFi vs. DeFi -- Comparing Centralized to Decentralized Finance.

Szabo, N. (1994). *Smart Contracts: Building Blocks for Digital Markets*. http://www.fon.hum.uva.nl

Szabo, N. (1997). *The idea of smart contracts*. http://szabo.best.vwh.net/smart_contracts_idea.html

Wang, S., Yuan, Y., Wang, X., Li, J., Qin, R., & Wang, F-Y. (2018). An Overview of Smart Contract: Architecture, Applications, and Future Trends. 2018 IEEE Intelligent Vehicles Symposium (IV). Changshu: IEEE.

Xu, J., Paruch, K., Cousaert, S., & Feng, Y. (2021). SoK: Decentralized Exchanges (DEX) with Automated Market Maker (AMM) Protocols. arXiv preprint arXiv:2103.12732.

Yaga, D., Mell, P., Roby, N., & Scarfone, K. (2019). Blockchain technology overview. arXiv preprint arXiv:1906.11078.

Zetzsche, D. A., Arner, W., & Buckley, R. P. (2020). Decentralized Finance. *Journal of Financial Regulation, 6*(2), 172–203.

DEVELOPMENT OF PROTOTYPE OIL PALM LOOSE FRUIT COLLECTOR

Napat Kamthonsiriwimol[1*], Hideo Hasegawa[2], Voravit Siripolawat[3], Kanokpanthon Logutarawong[4] and Sanon Boonmee[5]

[1,3]Faculty of Innovative Agriculture and Management, Panyapiwat Institute of Management
[2]Institute of Science and Technology, Niigata University
[4]Office of General Education, Panyapiwat Institute of Management
[5]Faculty of Agriculture at Kamphaengsaen, Kasetsart University
[*]**Corresponding Author, E-mail:** napatkam@pim.ac.th

Abstract

Loose fruits of oil palm (*Elaeis guineensis* Jacq.) played a crucial role in the oil extraction rate (OER) of palm oil industry. To maximize the OER and to minimize the risks of the uncollected oil palm fruits that could eventually grow up and turn into weed, the farmers need to collect all loose fruits from the plantation. However, it was tedious work that could lead to body fatigue and back pain in the workers. This research aimed to develop prototype oil palm loosen fruit collector in oil palm plantation. The prototype of oil palm loose fruit collector consisted of three main components as oval-shaped cases, transmission system and frame and supporting wheels was fabricated. Then, it was tested to evaluate the field performance by measuring the collecting capacity and the damage of the collected fruits compared with hand picking by labor at oil palm plantation in Nakorn Pathom province during February to May 2009. The results indicated that the collecting capacity of the prototype of oil palm loose fruit collector and hand picking was at 3.18 and 11.84 kg/hr, respectively. Moreover, the average percentage of damage of the collected fruits was 4.17 in oil palm loose fruit collector. Even if the efficiency of the oil palm loose fruit collector in terms of the collecting capacity and the damage of the collected fruits were lower than conventional method, the machine could be developed in the further.

Keywords: Oil palm, Loose fruit, Fruit collector

Introduction

Oil palm (*Elaeis guineensis* Jacq.) is a tropical perennial oil crop in the world that had an origin from West Africa. During the nineteenth century, oil palm seeds were transported from West Africa and introduced to the Dutch East Indies (modern Indonesia) and Malay State (modern Malaysia) as the newly introduced cash crops (Murphy, Goggin & Paterson, 2021). Then, it was brought to Thailand in1968 after the successful of growing in Malaysia (Wangrakdiskul & Yodpijit, 2015). The greatest palm oil producer, with a 59.7% share in the production in 2021, was Indonesia, followed by Malaysia (24.5%) and Thailand (3.8%) (Krungsri Research, 2022). For Thailand, oil palm is the prominent raw materials that broadly uses for cooking and renewable source of fuel (Somnuek, Slingerland, & Grunbuhel, 2016). The palm-oil-based biodiesel project was launched in Thailand in 2005 and had been intensively utilized as an alternative fuel for running machines and vehicles (Wangrakdiskul & Yodpijit, 2015). Approximately, 5.3-5.7 million liters per day of biodiesel would be required to use in Thailand according to the demand for diesel from the transport sector. Moreover, this strong domestic demand will annually increase by 4.0% (Krungsri research, 2021).

To meet the domestic demand of biodiesel, Thai government set the national policy to focus on additional productions of biodiesel from oil palm to support the program of promoting renewable energy. Consequently, the Thai Cabinet also approved the project to expand the oil palm plantation by aiming to increase the oil palm plantation area to 1.6 million Ha in 2029 (Keson & Wongsai, 2013). This encouraged many farmers to grow oil palm on their land even if their farms located in unsuitable areas such as the northern and northeastern of Thailand where the yields of oil palm production are low and not-cost effective according to the inappropriate climate conditions and insufficient rainfall (Kamthonsiriwimol et al, 2021).

Recently, the oil palm plantation significantly increased from 0.72 million Ha in 2013 to 1.01 million Ha in 2021. However, the yield of oil palm dramatically decreased from 0.53 tons per Ha in 2013 to 0.45 tons per Ha in 2021 (Office of Agricultural Economics, 2022). This decline in the yield of oil palm was mainly affected by climate change. An increasing temperature and insufficient rainfall had a direct impact to the yield of oil palm (Chankong et al., 2019).

Moreover, the oil extraction rate (OER) in Thailand is another factor that need to be taken in consideration for improving the palm oil industry. The OER of Thailand was around 16-17 % while the OER of neighboring countries such as Malaysia and Indonesia are around 20-24%. This low oil extraction rate stems partly from harvesting operation without concern of ripeness control. Some farmers may harvest the fresh fruit bunch (FFB) before the optimal ripening stage (Chucheep, Mahathaninwong, Limhengha, Petchi, &Templong, 2019; Junkwon et al., 2009a; Junkwon et al., 2009b).

Beside the optimal ripening stage of FFB, the neglection of oil palm loose fruits (LF) in the plantation usually occured as shown in Picture 1. The uncollected fruits were considered as another negative factor that reduced the OER since oil palm loose fruits are considered as one part of yield belong to FFB. Therefore, the oil palm plantation owner was suggested to collect the loose fruits that were left in the ground to minimize the reduction of OER (Yusoff et al., 2020; Shuib et al, 2018) Moreover, the uncollected fruits would eventually grow and turn into weed that need to be eliminated by chemical spraying (Picture 2) (Khalid, Shuib & Kamarudin, 2021). Therefore, the expansion of oil palm plantations is not the sole approach to increase the amount of palm oil in Thailand. The loose fruits collection may play an important role in increasing the OER. The more loose fruits were collected, the higher OER could be obtained. However, the loose fruits collection was labor-intensive work and could cause the risks in musculoskeletal disorder to the loose fruit collector due to extreme and repetitive posture during the work routines (Teo et al., 2021). Hence, the development of the machinery system to collect and manage the loose fruit may contribute to the appropriate way of loose fruit collection.

Picture 1: Loose fruits and FFB

Picture 2: Weed from uncollected fruits

Research Objectives

The objectives of this research were to develop prototype the oil palm loose fruit collector and evaluate the efficiency of the developed prototype compared to hand picking by man.

Literature Review

Oil palm is the highest oil-producing plant in the world. It is a monocotyledon belonging to the species *Elaeis* that could be classified into two species, so-called *Elaeis guineesis* and *Elaeis oleifera* (Sambanthamurthi, Sundram, &Tan, 2000). Generally, 4 to 6 million tons of crude palm oil (CPO) and 0.4 to 0.6 tons of palm kernel oil (PKO) can be produced from the mesocarp and endocarp of oil palm fruits per hectare per annum, respectively (Sunilkumar & Sparjan Babu, 2013). For the oil palm industry, the oil extraction rate is an important tool to indicate the profitability of the oil palm mill and oil palm plantations. To maximize the oil extraction rate , management of the plantation

respects to the optimum ripeness standard and loose fruit collection are the crucial factors that need to be concerned (Chang, Sani & Basran, 2003).

In the traditional oil palm harvesting, the farmer will count the loose fruits that fall on the ground and determine the maturity of the fresh fruit bunch. Commonly, the harvesting should be performed when there are 1 to 10 loose fruits on the ground (Khalid, Shuib & Kamarudin, 2021). The farmer will select the proper harvesting tools such as chisel or sickle to harvest the FFB as shown in Picture 3 (Corley &Tinker, 2003). The FFB will fall from the oil palm tree and some fruits may scattered on the ground according to the impact. The number of fallen fruits depends on the maturity of the FFB (Castillo, Rodriguez & Paez, 2017). Moreover, the oil palm loose fruits can be scattered around 1.5 to 2.5 m from the FFB impact point (Azali et al., 2015). Oil palm loose fruits generally have higher oil content than the fruits that attach to the FFB. The presence of oil palm loose fruits in the plantation comes from 2 sources. The first source comes from the fruits that are naturally detached from the FFB when start to ripe and ready to harvest. Another source is from the harvesting activity (Khalid, Shuib & Kamarudin, 2021). Most of loose fruits are from the outer diameter of the bunch that contain the highest oil content and contribute up to 40% of palm oil compared to other parts of spikelet (Henson, 2012). Therefore, the collecting of oil palm loose fruit is an important activity that cannot be neglected to increase the OER.

Oil palm loose fruits up to 62.5 kg/Ha/month could be left on the ground after the harvesting is done in Thailand (Khaehanchanpong et al., 2021). In general, the collection of oil palm loose fruits may be performed by the harvesters or by a separate group of female workers. To collect the oil palm loose fruits, the workers frequently bend down to collect the fruits that are scattered on the ground and move around from one oil palm tree to others. This may lead to body fatigue and back pain in the workers (Nur Syazwani et al., 2016).

To increase the productivity of oil palm loose fruit collecting, several types of oil palm loose fruit collector were developed such as roller type (Deraman, Shuib & Jaafar, 2009) and mechanicaltype (Shuib, et al., 2012; Khaehanchanpong et al., 2021). For roller type, it was designed to suit all types of field conditions. The user can operate the loose fruit collector by pushing the machine around the palm tree. A prototype (Picture 4 (a)) that was developed by Deraman, Shuib & Jaafar (2009) could collect the loose fruits around 30 to 60 kg/hr depending on the ground conditions. For the mechanical type, Shuib, et al (2012) aimed to increase the efficiency of loose fruit collector by using cyclonic vacuum to generate a constant suction power to suck the loose fruits from the ground. The trial revealed that the prototype (Picture 4 (b)) was capable of collecting the loose fruit between 252 to 306 kg/hr with the debris lower than 15 % and there was no damage or bruise on the fruits. A similar concept was also applied to develop the prototype (Picture 4 (c)) of Khaehanchanpong et al. (2021). The air suction type loose fruit collector was tested in the plantation. The results indicated that the loose fruits can be picked at 76.8 kg/hr by the machine. Therefore, the mechanical type of loose fruit collector demonstrated higher efficiency than the roller type. However, the cost of the mechanical type was also greater than the one of the roller type.

Picture 3: Harvesting of oil palm bunches from local plantation by using chisel in young oil palm

(a) Roller type
Deraman, Shuib & Jaafar (2009)

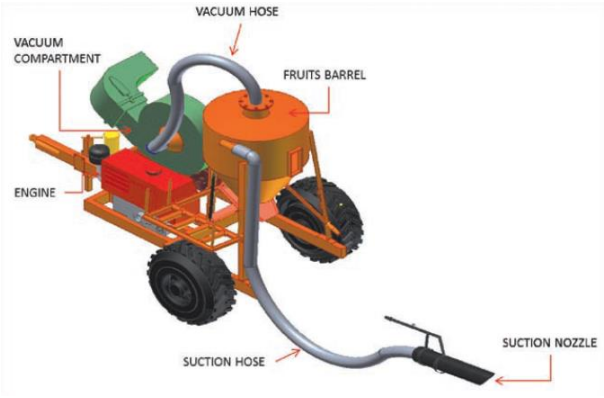

(b) Mechanical type
Shuib, et al (2012)

(c) Mechanical type
Khaehanchanpong et al. (2021)

Picture 4: Different types of oil palm loose fruit collector

Methodology

The loose fruit collector was developed by emphasizing the design criteria as safe and convenient to operate by a single operator, using the power source from gasoline engine, minimum maintenance and locally available spare parts. The prototype of the machine was fabricated as shown in Picture 5. It consisted of three main components as oval-shaped cases, transmission system and frame and supporting wheels as shown in Picture 6. To operate the loose fruit collector, the power of 5.5 HP four cylinders gasoline engine transmits the power through the gear box and pulley to move the oval-shaped cases. Then, the oval-shaped cases that are made of the spring rod will rotate with the pressure against the ground causing the rod of the cases to split open and to collect the loose fruit. Once the loose fruit is collected, the rod of the case will return to the normal position.

To examine the efficiency of loose fruit collector, a field trial was carried out for five replications at the oil palm plantation in Nakorn Pathom province compared to the loosen fruit collection by labor during February to May 2009 as shown in Picture 7. The no damage oil palm fruits were prepared and placed at the marked points around the oil palm trees at the experimental field at rate of 30 kg/Ha. Firstly, the hand picking by man were freely done by collecting the fruits to the bag. Then, the collected fruits were measured to calculate the collection capacity. The inspection of the damage of the fruits was also carried out to check the percentage of damaged fruits. To compare with hand picking, the loose fruit collector was operated in the experimental field and tested by the same manner as the hand picking by man. Finally, the collection capacity and percentage of damaged fruits of both loosen fruit collector and hand picking by man were calculated.

Picture 5: Oil Palm loose fruit collector

(a) oval-shaped cases

(b) transmission system (c) frame and supporting wheels

Picture 6: Three main components of oil palm loose fruit collector

Picture 7: Testing of oil palm loose fruit collector

Results

The results of the field trial were illustrated as in Table 1 and 2. The average loose fruit collecting capacity of oil palm fruit collector and hand picking were 3.18 and 11.84 kg/hr, respectively. The loose fruit collecting capacity of oil palm fruit collector was definitely lower than the one of hand picking by labor around 3.7 times. For the damage of oil palm loose fruits, the results revealed that the bruise was mostly found at the surface of the loose fruits in oil palm fruit collector as shown in Picture 8 while there was no damage fruit by hand picking method. The average percentage of damaged fruits of oil palm fruit collector was around 4.17 %.

Picture 8: Bruise of oil palm fruit causing by loose fruit collector

Table 1: A field test of oil palm loose fruit collector in comparison to hand picking by labor

Replication	Loose fruit collecting capacity (kg/hr)	
	Oil palm fruit collector	Hand picking by labor
1	3.52	13.37
2	2.95	11.55
3	3.15	10.28
4	3.46	11.36
5	2.82	12.62
Average	**3.18**	**11.84**

Table 2: Percentage of damage fruits by oil palm loose fruit collector

Replication	Damaged fruits (%)
1	4.63
2	4.24
3	3.57
4	3.99
5	4.44
Average	**4.17**

Discussion

The results of the field trial revealed that the efficiency of the developed oil palm loose fruit collector was lower than the one of handpicking method, this may be affected by the balance of the machine that was difficult to move in the plantation. The similar results were found in the study of

Khaehanchanpong et al. (2021) that the air-suction type oil palm loose fruit collector had the lower loose fruit collecting capacity than the one of hand picking method according to the difficulty of the operating with developed oil palm loose fruit collector. This may imply that the mobility of oil palm loose fruit collector must be concerned to improve the efficiency of the developed prototype. Moreover, the height of the grass in the plantation also affected the collecting capacity of roller type oil palm loose fruit collector as reported by Chanum (2012) and Deraman, Shuib & Jaafar (2009) that the ground conditions such as the types of surface and the height of grass were the factors that had strongly influence to the collecting capacity of roller type oil palm loose fruit collector. Therefore, it strongly recommended that the manager of the oil palm plantation should keep in mind that the proper management of grass in the plantation may assist to improve the efficiency of roller type oil palm loose fruit collector. For the damage of the collected fruit, the weight of the oil palm loose fruit collector needed to reduce to decrease the pressure that acted to rod of the oval-shaped cases.

Conclusion

In this study, the prototype of oil palm loose fruit collector was developed and tested to evaluate the efficiency compared to conventional method by hand picking in the oil palm plantation in Nakorn Pathom province. The conclusions are shown as follows:

(1) The prototype of developed machine was developed by using roller-type oil palm loose fruit collector. The field trials were done to compare the developed prototype with hand picking method by man. The loose fruit collecting capacity of the developed prototype was lower than that of the conventional method according to the balance of the machine and the difficulty to move around in the plantation.

(2) The damage of collected fruits was around 4.17% by using the prototype of oil palm loose fruit collector while no damage fruit presented in hand picking. The main causes of damage may come from the weight of the developed machine. Therefore, weight reduction of frame structure is suggested to take consideration for designing of the next model to minimize the damage.

References

Azali, A., Syed, S.S.A, Abdul, H.A.A. & Azahah, A. (2015). Conceptual of mobile oil palm fresh fruit bunch catcher. *International Journal of Agriculture Innovation and Research, 4*(6),1159-1163.

Bandita, Y. (2007). *Ten Million Rai of Oil Palm Plantation: A Catastrophe for the Thai People.*

Castillo, E.G., Rodriguez, L.F. & Paez, A.F. (2017). Evaluation of Two Harvesting Procedures for Oil Palm (*Elaeis guineensis* Jacq.) Fruits: A Case Study. *Agronomia Colombiana, 35*(1), 92-99.

Chang, L.C., Sani, A.R.A. & Basran, Z. (2003). An Economic Perspective of Oil Extraction Rate in the Oil Palm Industry of Malaysia. *Oil Palm Industry Economic Journal*, 3, 25-31.

Changkong, J., Sittisutikul, K., Sinnarong, N. & Autchariyapanitkul, K. (2019). Impact of Climate Change on Oil Palm Production in Southern Thailand. *Journal of Rajamangala University of Technology Srivijaya, 11*(1), 54-66.

Chanum,V. (2012). *Development of Roller-type Electrical Oil Palm Loose Fruit Collector*. Special Problem, Kasetsart University, Thailand.

Chucheep, T., Mahathaninwong, N., Limhengha, S., Petchi, D. & Templong, P. (2019). Ripeness Inspection of Oil Palm Fruits by Applying Hardness Test Technique. *The 16th ASEAN Food Conference (16th AFC 2019)*. (pp. 279-283). October 15-18, 2019. Bali: Indonesia.

Corley, R.H.V & Tinker, P.B. (2003). *The oil palm (4th ed.).* Massachusetts: Blackwell Science Ltd.

Deraman, M. S., Shuib, A. R. & Jaafar, M. S. (2009). *Roller-type Oil Palm Loose Fruit Picker*. Retrieved April 10, 2023, from http://palmoilis.mpob.gov.my/publications/TOT/TT-419.pdf

Hensen, I.E. (2012). *Palm Oil: Production, Processing, Characterization and Uses*. Illinois: AOCS Press.

Junkwon, P., Takigawa, T., Okamoto, H., Hasegawa, H., Koike, M., Sakai, K., Siruntawineti, J., Chaeychomsri, W., Sanevas, N., Tittinuchanon, P. & Bahalayodhin, B. (2009a). Potential Application of Color and Hyperspectral images for Estimation of Weight and Ripeness of Oil Palm (Elaeis guineensis Jacq. var. tenera.). *Agricultural Information Research, 18*(2), 72-81.

Junkwon, P., Takigawa, T., Okamoto, H., Hasegawa, H., Koike, M., Sakai, K., Siruntawineti, J., Chaeychomsri, W., Vanavichit, A., Tittinuchanon, P. & Bahalayodhin, B. (2009b). Hyperspectral Imaging for Nondestructive Determination of Internal Qualities for Oil Palm (Elaeis guineensis Jacq. var. tenera.). *Agricultural Information Research, 18*(3), 130-141.

Keson, J. & Wongsai, S. (2013). Oil palm expansion in Amphoe Lam Thap, Krabi province, Thailand. *Proceedings of the 1st Annual PSU Phuket International Conference 2012.* January 10-12, 2013. Phuket: Thailand.

Khaehanchanpong, Y., Suttiwaree, P., Sukpraset, W, Taikonthong, P., Sngiamphongse, S. & Senanarong, A. (2021). Research and Development of Oil Palm Loose Fruit Collecting Machine. *Thai Agricultural Research Journal*. 39(1), 87-95.

Khalid, M.R., Shuib, A.R. & Kamarudin, N. (2021). Mechanising Oil Palm Loose fFruits Collection: A Review. *Journal of Oil Palm Research*, 33 (1), 1-11.

Krungsri Research. (2021). *Industry Outlook 2021-2023: Biodiesel*. Retrieved April 20, 2023, from https://www.krungsri.com/en/research/industry/industry-outlook/energy-utilities/biodiesel/io/io-biodiesel-21.

Krungsri Research. (2022). *Industry Outlook 2022-2024: Palm Oil Industry*. Retrieved April 25, 2023, from https://www.krungsri.com/en/research/industry/industry-outlook/agriculture/palm-oil/IO/Oil-palm-industry-2022-2024.

Murphy, D.J., Goggin, K. & Paterson, R.R.M. (2021). Oil Palm in the 2020s and Beyond: Challenges and Solutions. *CABI Agriculture and Bioscience*, 39(2),1-22.

Napat, K., Chunnasit, B., Hasegawa, H. & Luangvasuwat, S. Classification of Oil Palm Fruit on Ripening Stage Using Universal Testing Machine. *Proceedings of The 11th National and the 5th International PIM Conference 2021*. July 16, 2021. Nontaburi, Thailand.

Nur Syazwani, M.N., Baba, M.D., Mohd Nizam, A.R., Ezrin, H.,S. & Norani, N. (2016). Malay Oil Palm Workers Are in Pain: Hazard Identification and Ergonomics Related Problems. *Malaysian Journal of Public Health Medicine*. 16(1), 50-57.

Office of Agricultural Economics. (2022). *Agricultural Statistics of Thailand 2020*. Retrieved April 25, 2023, from https://www.oae.go.th/assets/portals/1/files/jounal/2566/yearbook2565.pdf.

Sambanthamurthi, R., Sundram, K. & Tan, Y.A. (2000). *Chemistry and Biochemistry of Palm Oil. Progress in Lipid Research, 39*, 507-558.

Shuib, A.R., Khalid, M.R., Bakri, M.A.M., Deraman, M.S. & Kamarudin, N. (2018). Development of Oil Palm Loose Fruit Collecting Machine with Elevated Discharge Mechanism (Mark III). *International Journal of Engineering Research & Technology*, 7(10), 225-234.

Shuib,A.R., Khalid, M.R., Deraman, M.S. & Mohamed, A. (2012). *Oil Palm Loose Fruits Collector (MK III)*. Retrieved April 14, 2023, from http://palmoilis.mpob.gov.my/publications/TOT/TT-505.pdf

Somnuek, S., Slingerland, M. M.A. & Grunbuhel, C.M. (2016). The Introduction of Oil Palm in Northeast Thailand: a New Cash Crop for Smallholders? *Asia Pacific Viewpoint, 57*(1), 76-90.

Sunilkumar, K & Sparjan Babu, D.S. (2013). Surface Color Based Prediction of Oil Content in Oil Palm (*Elaeis guineensis* Jacq.) fresh fruit bunch. *African Journal of Agricultural Research, 8*(6), 564-569.

Teo, Y.X., Chan, Y.S., Gouwanda, D., Gopalai, A.A., Nurzaman, S.G. & Thannirmalai, S. (2021). Quantification of Muscles Activations and Joints Range of Motions During Oil Palm Fresh Fruit Bunch Harvesting and Loose Fruit Collection. *Scientific Reports*, Retrieved April 10, 2023, from https://doi.org/10.1038/s41598-021-94268-4.

Wangrakdiskul, U. & Yodpijit, N. (2015). Trends Analysis and Future of Sustainable Palm Oil in Thailand. *King Monkut's University of Applied Science and Technology, 8*(1), 21-32.

Yusoff, M.Z.M., Zamri, A., Abd Kadir, M.Z.A., Wan Hassan, W.Z. & Azis, N. (2020). Development of integrated loose fruit collector machine for oil palm plantations. *Bulletin of Electrical Engineering and Informatics*, *9*(2), 500-506.

EFFECTS OF TEMPERATURES AND PACKAGING ON STORAGE LIFE AND QUALITIES OF ICE PLANT (*Mesembryanthemum crystallinum* L.)

Chairat Burana[1*], Voravit Siripholvat[2], and Inna Martha Rumainum[3]

[1,2]Faculty of Innovative Agriculture and Management, Panyapiwat Institute of Management
[3]Faculty of Agriculture, University of Papua
[*]**Corresponding Author, E-mail:** chairatbur@pim.ac.th

Abstract

The objective of this research study to the effects of temperatures and packaging on maintain the quality and storage life of ice plant (*Mesembryanthemum crystallinum* L.). Fresh Ice Plant were store at different temperature; 25 °C (Control), 4, 10 and 13 °C, respectively. The result found that storage temperatures at 4, 10 and 13 °C maintained the qualities by decreased the respiration rate and ethylene production compared with the control. These storage temperatures (4, 10 and 13 °C) reduced color changed due to delayed the reducing of Chlorophyll a, Chlorophyll b and total Chlorophyll. Moreover, the decreasing of antioxidant (DPPH) was also delayed. Storage at 4 °C prolonged the storage life for 10 days, while at 10 °C as well as 13 °C prolonged the storage life for 6 days, while the storage life of 2 days was observed in control treatment (25 °C).

These results indicated that the optimize temperature for storage the Ice Plant was 4 °C. The effect of packaging types combined with the optimum temperature (4°C) were investigated. The packaging types including Zip bag, Plastic box and Biodegradable Plastic box compared with the control (Clamshell). All packaging types combined with storage at 4°C prolonged the storage life of Ice Plant for 10 days. While, the external characteristics and internal qualities were constant throughout the storage period and no different among the packaging types. Whereas, vitamin C content gradually decreased throughout the storage life. All of above results indicated that, due to no different among the packaging types so selection the packaging type should depend on the convenient, beautiful, function and cost.

Keywords: Ice Plant, temperature, Quality, Storage Life

Introduction

Ice plant (*Mesembryanthemum crystallinum* L.) is a salt-accumulating halophyte native to Namib Desert on the western coast of southern Africa and became leafy vegetable (Winter, 1978) Ice plant are a good natural source of nutrients, minerals, and phytochemicals, which may improve human health. To enhance local vegetable production, recently we have successfully grown in Thailand using an indoor hydroponic farming system with adequate water supply under light emitting diodes (LEDs) lighting or Plant Factory with Artificial Light (PFAL) and organic system (Chairat et al., 2020).

Recently, ice plant is becoming a popular and high potential crop in Thailand. However, ice plant is perishable vegetable due to high respiration, high ethylene and have high moisture content effect on easy to bruise (perishable product). The use of postharvest technology especially low temperatures to retard senescence has been well reported for a variety of vegetables and fruits (Kader and Ben-Yehoshua, 2000). However, there are no report on maintain the quality of ice plant.

This study evaluated respiration rate, ethylene production rate, DDPH, chlorophyll a, b and total chlorophyll content during storage after treat with different temperature. Then the optimize temperature apply with different packaging type to maintain the quality of fresh ice plant.

Research Objectives

The objective of this research was to investigate the effect of low temperature treatments and packaging types on the quality and storage life of fresh ice plant.

Literature Review

Ice plant is already being consumed as an edible plant in several countries, such as Japan, India, America, Australia, and New Zealand, and in several countries in Europe (Agarie et al., 2007). This species is high-value added crops have also become widely consume in Thailand. This plant has high tolerance to drought, low temperature and salinity (Adams et al., 1998). As features of the ice plant, it forms bladder cells on leaf and stem surfaces. Bladder cells have useful phytochemical contents to humans, such as phenolic compounds, myo-inositol, pinitol, and several minerals.

Ice plant have very short life at ambient due to wilting and bruised. Temperature is an important factor of postharvest processing and responsible for respiration and water activity of agricultural produces both; fruits and vegetables. High temperature accelerates the respiration rate and spoiled the perishable fruits and vegetable rapidly due to high water activity in the comparison of the agriculture produces have less water activity. Refrigerated storage can delay the senescence symptoms in perishable crops such as delay ripening, softening, and textural and color changes. One of the most important functions of refrigeration is to control the crop's respiration rate and ethylene production (Hardenburg et.al., 1986)

Packaging should be designed to prevent physical damage to produce, and be easy to handle. Modified atmosphere packaging (MAP) is one common package methods in postharvest storage and shelf-life, which maintain a high carbon dioxide (CO_2) and low oxygen (O_2) concentrations gas environment in the package, resulting in to repress of respiration rate (Qu et al., 2022). MAP delays fruit ripening and maintain quality by inhibiting fruit physiological activities, microbial spoilage and water loss, significantly prolong the storage and shelf-life for various fruit and vegetable (Cai et al., 2022, Qu et al., 2022). However, the unsuitable higher CO_2 or low O_2 concentration could develop an undesirable taste in raspberries and strawberries (Van der Steen et al., 2002). The combination MAP with other treatment such as 1-methylcyclopropent (1-MCP) and low temperature treatments might show better effects on quality control than MAP alone (Chairat et al., 2014; Chairat, 2018). For example, the combined treatment of a gaseous ozone and MAP pre-treatment extend the postharvest storage of small berry fruit (Pinto et al., 2020). During the low temperature storage, MAP and 1-MCP reduced the chilling injury symptom of sweet persimmon (Zhao et al., 2020).

Methodology

Plant Materials

Fresh Ice Plant (*M. crystallinum)* were purchased from commercial grower in Phisanulok Province (16°49'29.32"N, 100°15'30.89"E), Thailand. Ice Plant were harvested in the morning at commercial stage then taken to laboratory at Panyapiwat Institute of Management, Nonthaburi Province within 6 hrs. by controlled temperature transportation. The samples were selected based on uniformity in color and size, and absence of visual defects.

Figure 1: The commercial stage of Ice Plant (*M. crystallinum)*

Effect of temperature on postharvest quality of ice plant

One hundred grams (g) of samples were packed in the polypropylene (PP) box (12.0 x 17.2 x 6.5 cm.) then cover with the lid. After that, the boxes were separated hold at different temperature including 25 ℃ (Control), 4, 10 and 13 ℃, respectively. The data recording were respiration rate, ethylene production rate, DPPH radical scavenging activity, chlorophyll a, b and total chlorophyll content, in every 2 days of storage time.

Effect of packaging type on shelf life of ice plant

The sample 100 g were pack in different packaging including Clamshell (12.0 x 17.2 x 6.5 cm.), Zip bag (18.0 x 28.0 cm.), Plastic box (12.0 x 17.2 x 6.5 cm.) and Biodegradable Plastic box (12.0 x 17.2 x 6.5 cm). All packaging of samples were kept at 4°C and 60±2% Relative Humidity (RH). The shelf life of samples were consider by wilting, leave yellowing, bruise and injuries symptoms, in every 2 days of storage time.

Statistical analysis

All treatments were performed in triplicate. The data were subject to analysis of variance (ANOVA) and mean values were compared using SAS program.

Results and Discussion

Respiration rate

The comparison of respiration rate from different temperature treatments during storage showed in Figure 2. Immediately after treatment, there were no differences in respiration rate between control and treated ice plant. During storage time at all temperature respiration rate increased, especially at 25°C is higher than low temperature and the shelf life was finished on 4 days. The respiration rate of ice plant were significant different among treatment from day 6 until the end of experiment. The lowest of respiration was found in ice plant storage at 4°C. This work were in accordance with Hardenburg (1986) who found precooling or storage could preserve product quality and increases the shelf life by reduce enzyme activity, respiration rate, reduce ethylene production and slowing the rate of water loss.

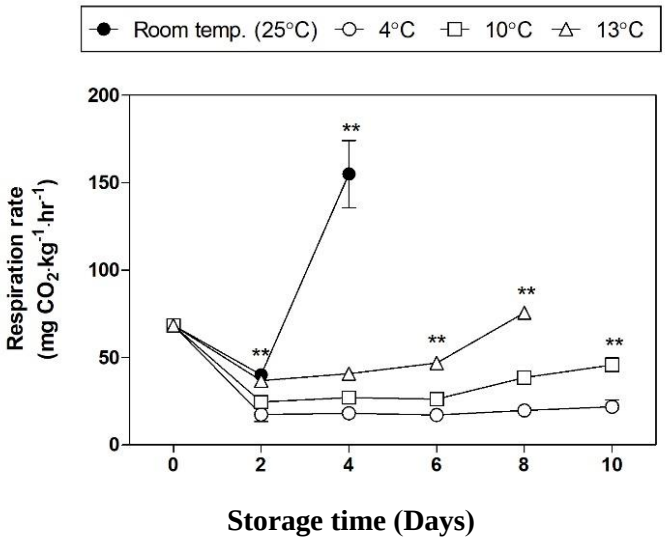

Figure 2: Respiration rate of ice plant at different temperature during storage

Ethylene production

Ethylene production rate was significantly (P≤0.05) affected by low temperature storage compared with 25°C. The 25°C ice plant showed highest ethylene production rate on day 2 and day 4 after storage (Figure 3). Ice plant stored at 4 °C show lowest ethylene production from day 4 until the end of experiment. Similar with Kader (2002) reported that ethylene production rates increase with maturity at harvest and with physical injuries, increase temperatures up to 30°C. On the other hand, ethylene production rate by fresh horticultural crop are reduce by storage at low temperature.

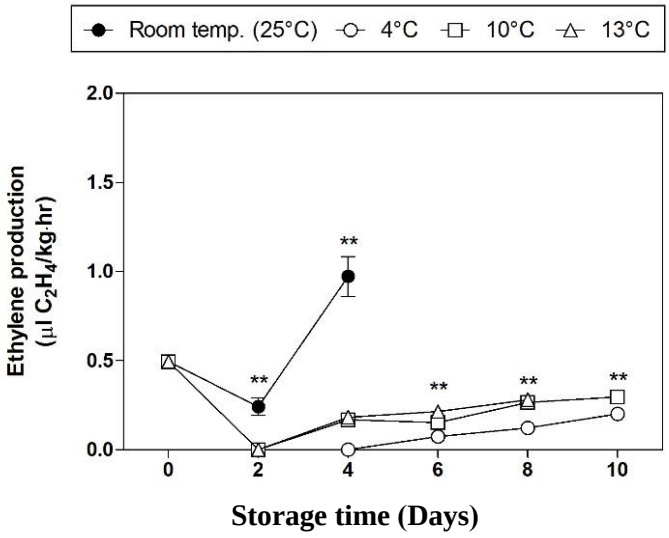

Figure 3: Ethylene production of ice plant at different temperature during storage

DPPH radical scavenging activity

The DPPH radical scavenging activity in all treatments of ice plant slightly decrease from day 2 after harvest. In the control, show lowest DPPH radical scavenging activity on day 4 as 1.66 mM TEAC/ g FW. The ice plant treated with 4°C show highest DPPH radical scavenging activity and significant highest on day 6 as 2.75 mM TEAC/ g FW (Figure 4).

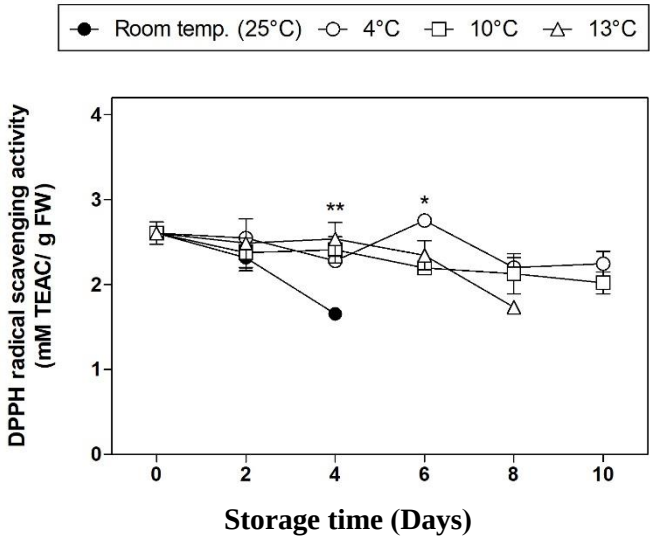

Figure 4: DPPH radical scavenging activity of ice plant at different temperature during storage

Chlorophyll a, b and total chlorophyll content

The changes in chlorophyll a, b and total chlorophyll in ice plant stored at different low temperatures (4, 10 and 13 °C) were determined. All treatments reduced color changed due to delayed the reducing of Chlorophyll a, Chlorophyll b and total Chlorophyll compared with the control at 25 °C (Figure 5). During chlorophyll degradation in plants, chlorophyll a transformed to chlorophyllide a stimulating the action by chlorophyllase enzyme (Hortensteiner, 1999; Matile et al., 1999). Chlorophyllide a is then acted by the enzyme Mg-dechelatase removing Mg^{2+} from the molecule and forming pheophorbide a, consequently the green color is lost (Matile, 1980; Fumamoto et al., 2002).

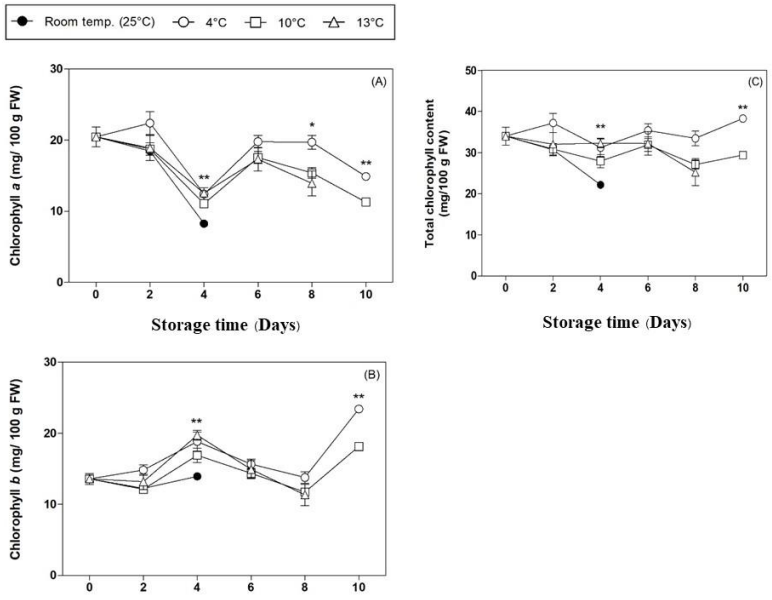

Figure 5: Chrolophyll a, b and total chrolophyll of ice plant at different temperature during storage

Packaging is effective in prolonging the shelf life of horticultural products by decreasing oxygen (O_2) and increasing carbon dioxide (CO_2) concentration in the atmosphere. However, regarding effect of packaging type on shelf life of ice plant, there were no different among the treatments throughout the experiment periods. (Data not shown)

Conclusion

From the results of this experiment proved that, fresh ice plant (*M. crystallinum)* should be store under low temperatures (4, 10 and 13 °C) because reduced respiration rate, ethylene production and delayed the color change result as maintained the quality and prolong the shelf life. However, in order to maintain quality after harvest it is essential that low temperature combine with appropriate packaging to remain relative humidity (RH) appropriately.

References

Adams, P., Nelson, D.E., Yamada, S., Chmara, W., Jensen, R.G., Bohnert, H.J. and Griffiths, H. (1998). Growth and development of *Mesembryanthemum crystallinum* (Aizoaceae) . *New Phytol*. 138 : 171-190.

Agarie, S., Shimoda, T., Shimizu, Y., Baumann, K., Sunagawa, H., Kondo, A., Ueno, O., Nakahara, T., Nose, A. and Cushman, J.C. (2007). Salt tolerance, salt accumulation, and ionic homeostasis in an epidermal bladder-cell-less mutant of the common ice plant *Mesembryanthemum crystallinum*. J. Exp. Bot. 58: 1957-1967.

Burana, C., T. Kurokura, Y. Yamaki and K. Yamane, (2014), Modified atmosphere (MA) and 1-methylcyclopropene (1-MCP) combination treatment extends the postharvest life of carnations, *Environmental Control in Biology, 52* (3), 131-136.

Chairat Burana (2018) , Effect of pre-cooling treatment, 1-methylcyclopropene (1-MCP) and controlled atmosphere (CA) on vase life of cut spray carnation flowers, *International Scientific Journal of Engineering and Technology (ISJET), 2*(2), 33-37.

Funamoto, Y., Yamauchi, N., Shigenaga, T. and Shigyo, M. (2002). Effects of heat treatment on chlorophyll degrading enzymes in stored broccoli (*Brassica olearacea* L.), Postharvest Biology and Technology 24: 163-170.

Hardenburg, Robert, (1986) The Commercial Storage of Fruits, Vegetables, and Florist and Nursery Stocks. USDA Handbook No. 66. United States Department of Agriculture, *Agricultural Research Service*. 136 p.

Hortensteiner, S. (1999). Chlorophyll breakdown in higher plants and algae, Cellular and Molecular Life Science 56: 330-347.

Kader, A, A., (2002), Postharvest biology and technology: an overview. In: 'Postharvest Technology of Horticultural Crops'; pp. 39-47. Ed; A.A. Kader, University of California, Agricultural and Natural Resources, Publication 3311, pp.535.

Matile, P. 1980. Catabolism of chlorophyll, Involvement of peroxidase, Z. Pflanzenphysiol 99: 475-478.

Matile, P., Hortensteiner, S. and Thomas, H. 1999. Chlorophyll degradation. Annual Review of Plant Physiology and Plant Molecular Biology 50: 67-95.

Winter, K. (1978). Phosphoenolpyruvate carboxylase from *Mesembryanthemum crystallinum*: its isolation and inactivation in vitro. *Journal of Experimental Botany* 29: 539–546.

PHYSICAL PROPERTIES, CHEMICAL PROPERTIES AND BIOLOGICAL OF BIODEGRADABLE PACKAGING FROM DRY RICE STRAW

Korawit Chaisu

Faculty of Innovative Agriculture and Management
Panyapiwat Institute of Management, Thailand
Corresponding Author, E-mail: Korawitchaisu@gmail.com, Korawitchai@pim.ac.th

ABSTRACT

These Global rice productions in 2021/22 is forecast at a record 506.6 million tons (milled basis). The 6th was Thailand, 18,600,000 tonnes. Thailand became the world's third-largest rice exporter by shipping 6.12 million tonnes of rice on 2020. Moreover, 49% of rice is rice straw that mean agriculture wastes. Noremorely, farmer always burn dry rice straw that become to air pollution. This sentence is not showed the reasonable or importance of rice straw. Rice straw have been identified and used to make biodegradable food containers, biodegradable packaging medical products, and biodegradable industrial packaging products. Therefore, this research was studied and developed a new eco-friendly biodegradable packaging from dry rice straw from Thailand. The methods for analysis including Physical, Chemical and Biological analysis. The results as size 12.7x20.32 cm2, thickness 1.33 mm., weight 20 mm., color was brown, tensile strength (n=3) was 15.89 Mpa. Zinc was 59.29 mg/kg; Copper was 15.17 mg/kg. and without colony on nutrient agar (NA) incubated at 37◦C, 24 hrs. Therefore, this research a new eco-friendly biodegradable packaging from dry rice straw can be add values of agriculture wastes, reduce chemical (without sodium hydroxide) on process and more sustainability. Future study will be applying to food and non-food industries and promote to publication using.

Keywords: Biodegradable packaging, Dry Rice Straw, Eco-friendly

Introduction

Global rice production in 2021/22 is forecast at a record 506.6 million tons (milled basis) [1]. United States Department of Agriculture (USDA) estimated Global Rice Production of 2020/2021, The 6th was Thailand, 18,600,000 tonnes [2]. Thailand became the world's third-largest rice exporter by shipping 6.12 million tonnes of rice on 2020, up 6.7 per cent year on year [3]. Moreover, 49% of rice is rice straw that mean agriculture wastes. Noremorely, farmer always burn dry rice straw that become to air pollution. Cellulose fibers of rice straw have been identified and used to make biodegradable food containers, biodegradable packaging medical products, and biodegradable industrial packaging products. Technology adaption of rice straw processing seems to have potential to be further commercialized [4-6]. Recently, there has been an increasing trend of using paper as packaging, resulting in the development of paper produced from natural fibers. The effective utilization of byproducts, by translating waste and byproducts into beneficial resources through technological approaches, has been reported to increase the sustainable development of economic value and reduce environmental pollution [7]. Normally used NaOH in process condition (laboratory scale) for the separation of cellulose from rice straw Therefore, this research was studied and developed a new eco-friendly biodegradable packaging (without sodium hydroxide) from dry rice straw from Thailand.

Research Objective

This research was studied and developed a eco-friendly biodegradable packaging from dry rice straw in Thailand.

Literature Review

Nowadays, the largest part of materials used in packaging industries is based on synthetic plastics with a production of more than 200 million tones/year and annual growth of approximately 5%, which represents the largest field of crude oil utilization. The degradation is fast only if the three requirements are present. Generally, biodegradation occurs at very low rate at home or in a supermarket in comparison to compost medium. In compost medium, bio-plastics are converted into biomass, water, and CO_2 in 6–12 weeks. Natural polymers such as rubber, lignin, and natural fibers and synthetic polymer like polyolefin are degraded by oxo-biodegradation mechanism and consequently cannot satisfy the rapid mineralization criteria required for standard biodegradation (Picture. 1) [6].

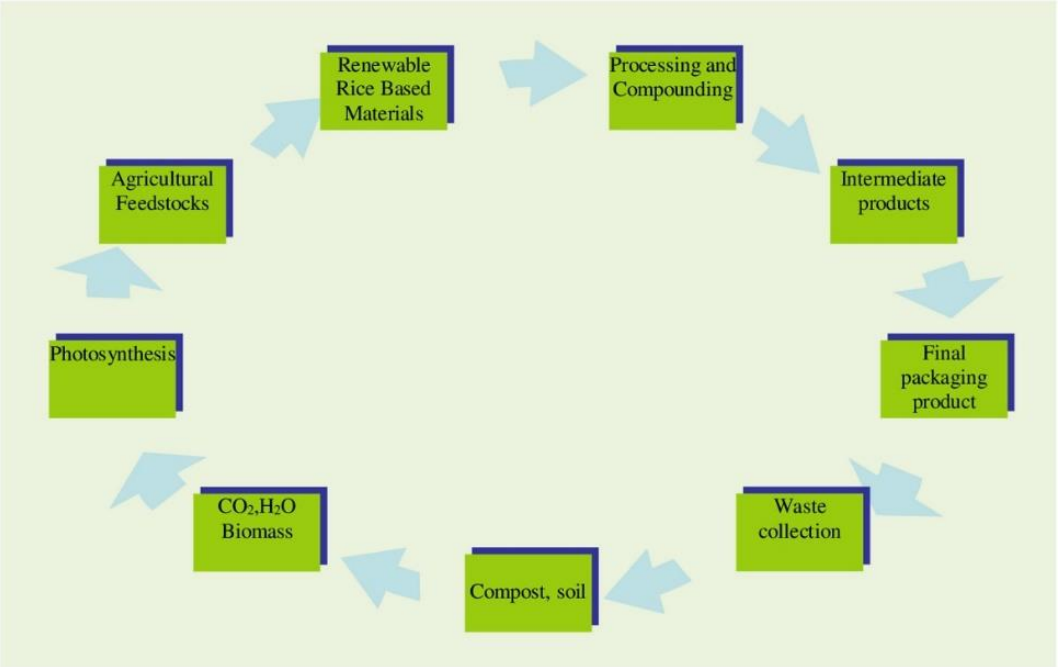

Picture 1: A typical life cycle of rice waste–based packaging materials [6].

Rice straw availability

Since 6500 BC, rice has been widely cultivated in various parts of the world and more dominantly in Asian countries. China, India, Indonesia, Bangladesh, Vietnam, Thailand, Myanmar, Philippines, Brazil, and Japan are among the top 10 rice-cultivating countries in the world [8-9]. Rice straw, which is sometimes regarded as solid waste from rice cultivation, is generated in huge quantities worldwide. The overall biomass of the rice straw is determined by several factors, including rice variety, fertilizer management, and soil and climatic conditions [10]. The harvesting method also determines how much rice straw is left behind in the field, as the height of crop cutting varies with harvesting methods. The paddy to straw ratio lies in the range of 0.74 to 4.3 [11-12]. Total straw biomass yield ranges between 7.5 to 8 t/ha. (Picture 2)

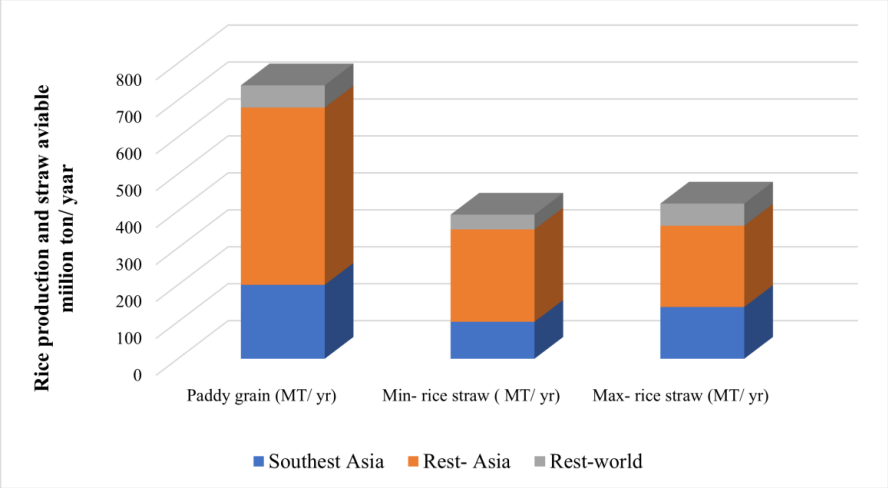

Picture 2: Production of rice straw around the world [12-13]

Composition of Rice Straw

Rice straw is a tenacious part of the rice plant whose cell walls are naturally designed to meet various growth needs, including protection from extreme weather conditions, insects, and viruses. Rice straw consists of structural components such as cellulose (33 to 47%), hemicellulose (19 to 27%), lignin (5 to 27%), silica (both acid- soluble and insoluble), and other non-silica oxides. Rice straw also has other organic components including proteins (approximately 3%), pectins (2.8%), free sugars, chlorophyll, lipids, oils, and waxes. Proximate analysis of rice straw, wheat straw, sugarcane bagasse, and corn stover reveals that ash percentages are 7.8 to 20.3%, 5.2 to 10.5%, 0.9 to 11.5%, and 2.65 to 10.5%, respectively. Based on these amounts, rice straw has higher ash percentage compared to other agricultural residues [13-23].

Nanocellulose Definition and Classification

Nanotechnology is an interdisciplinary science that combines mathematics, physics, and chemistry to create tiny particles having at least one dimension in the nanoscale range (1 to 100 nm) [24]. Cellulose is a biopolymer with linear homo- polysaccharide composed of D-glucopyranose units joined together by α (1–4) linkages with a repeating unit of cellobiose [25,13]. Nanocellulose is composed of two regions, crystalline and amorphous, of which the crystalline region is responsible for strength and stiffness, while the amorphous region provides good flexibility to the plant cells (Picture 3.).

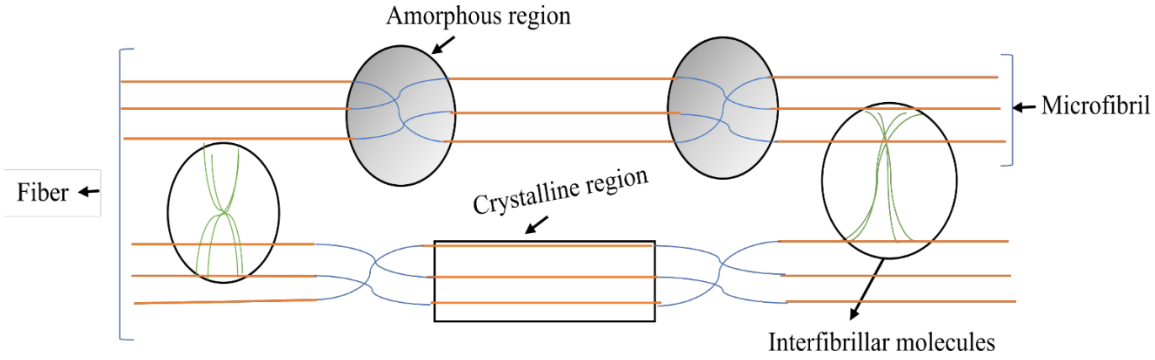

Picture 3: Crystalline and amorphous region of cellulose fiber [25,13]

Production of Nanocellulose from Rice Straw

Production of nanocellulose (NC) from rice straw includes a variety of pre-treatment methods including separation of lignin and hemicellulose. Stepwise procedures for their preparation, as adopted and presented in past studies, includes: (i) separation of cellulose fiber from rice straw, (ii) pretreatment of separated cellulose fibers, and (iii) mechanical isolation of NC through an energy-efficient [25,13], are discussed in the following sections. The production and separation of nanocellulose and nanocrystals from rice straw are shown in detail in Picture 4 and 5, respectively.

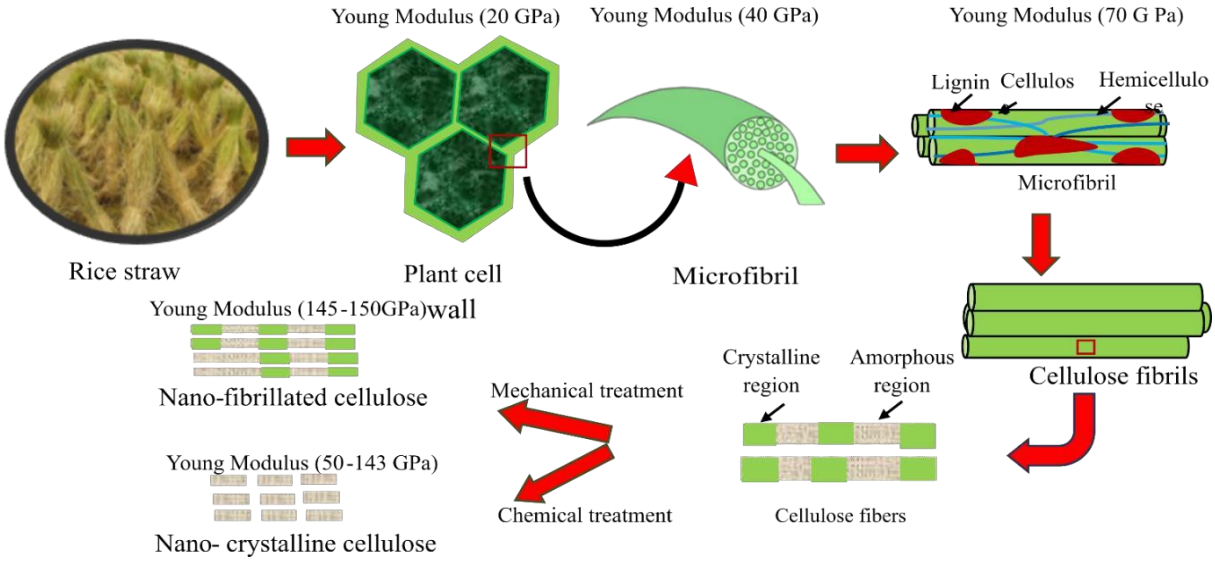

Picture 4: Production of NC and CNCs from rice straw [25,13]

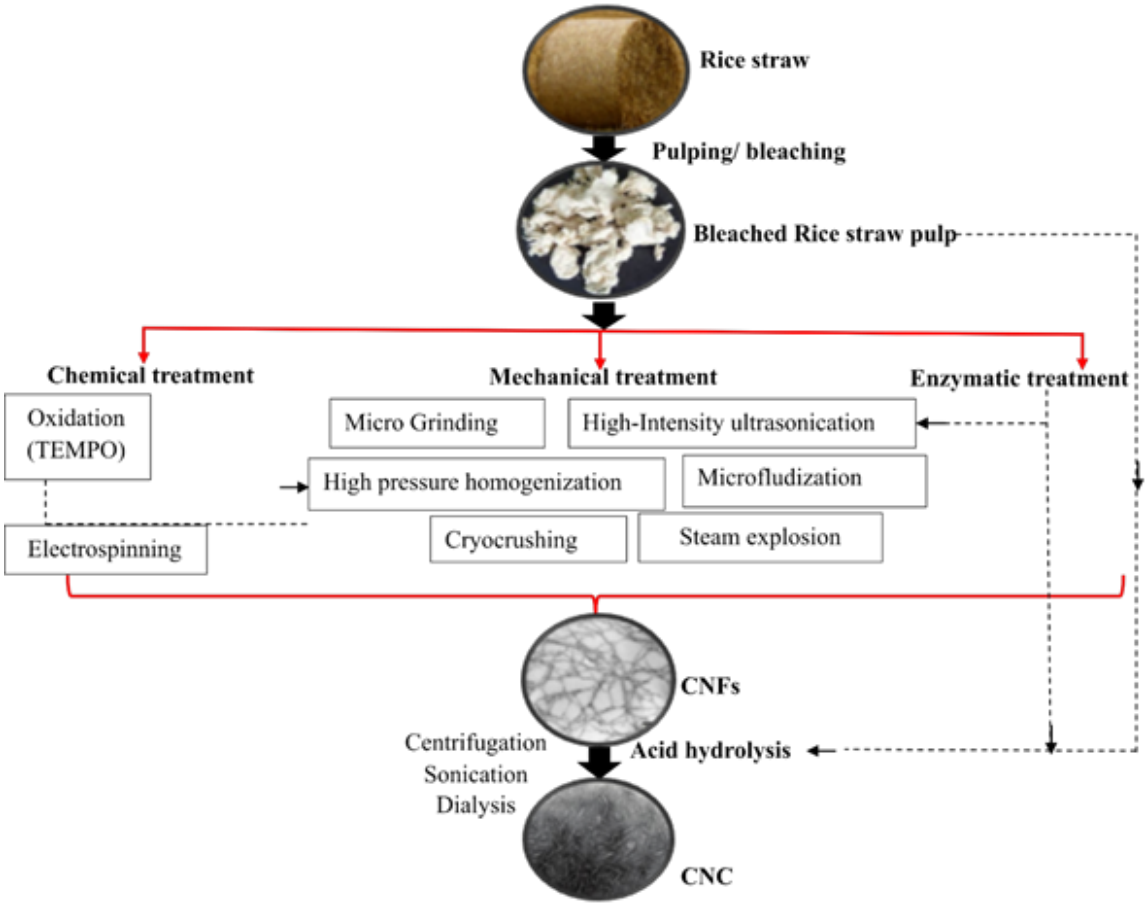

Picture 5: Full schematic diagram for the production of NC and CNCs [25,13]

Separation of Cellulose Fiber

Separation of rice straw cellulose, the primary step of nanocellulose preparation involves the pulping treatment desired to collect cellulose and remove lignin from the rice straw biomass. Different alkaline and organosolv pulping methods are used for separating cellulosic fibers from rice straw. The detailed process conditions, characteristics of obtained pulp, and paper properties of obtained pulp are summarized, normally used NaOH in process condition (laboratory scale) for the separation of cellulose from rice straw [26-32,13]

Recently, there has been an increasing trend of using paper as packaging, resulting in the development of paper produced from natural fibers. The effective utilization of byproducts, by translating waste and byproducts into beneficial resources through technological approaches, has been reported to increase the sustainable development of economic value and reduce environmental pollution [7].

Methodology

A. Materials preparation

A 1.1 Dry rice straw preparation: the dry rice straw from jasmine rice; Hom Mali rice from Phayao (700 g.) was cut into a size of 3cm. mix with A4 paper (300) respectively. Then, immersed in water within 24 hours. After that, all samples were boiled at 100 ◦C within 8 hours and move to dry process (without sodium hydroxide). Whereupon, all samples were grind with a stainless steel electric

grinder (2400 w, 28,000 r/m) for 10 s. Moreover, all martials were immersed in water (5000 mL.) for make a rice straw paper sheets size A4 (21x29.7 cm^2)

A1.2 biodegradable packaging preparation, the rice straw papers were prepared to size 15.24x22.86 cm2 for 4 sheets (thick 2 mm.). Sprinkle about 5 mL. of water onto the paper surface. Then, put into the packaging machine (500 w) at 140 ๐C within 1 min. waiting for room temperature (30 ๐C) and cutting sample to size 12.7x20.32 cm2.

B. Physical, chemical and biological analysis for a eco-friendly biodegradable packaging from dry rice straw

B1.1 Physical analysis

Using biodegradable packaging sample size 12.7x20.32 cm^2 to tested by Tensile Strength tester and Tensile strength = F/(WxT) Mpa; F= Force greatest force causing the test piece to break (N), W= width of test specimen (mm.), T= thickness of test specimen (mm.) applied from Soraya, 2014 [5].

B2.2 Chemical analysis

The biodegradable packaging from dry rice straw were tested Zinc (Zn), Copper (Cu) by Diethylene Triamine Penta Acetic Acid (DTPA) respectively, applied from Salwinder S. D. et al., 2021 [8].

B2.3 Biological analysis

The biodegradable packaging from dry rice straw were tested under UV light within 30 min. after that using loop swab on sample surface to nutrient agar (NA) incubated at 37 ๐C, 24 hrs.

Results

The results found that physical, chemical and biological properties follow by the results as size 12.7x20.32 cm^2, that size is not result. thickness 1.33 mm., weight 20 mg., color was brown, without flavor, tensile strength (n=3) was 15.89 Mpa. Zinc was 59.29 mg/kg, Copper was 15.17 mg/kg. and without colony on nutrient agar (NA) incubated at 37 ๐C, 24 hrs. (Picture. 6-8, Table 1).

Picture 6: A eco-friendly biodegradable packaging from dry rice straw, size 12.7x20.32 cm^2

Picture 7: The results of physical analysis

Table 1: The results of physical, chemical, biological analysis

No	Physical analysis	Results (n=3)
1	Size (cm^2)	12.7x20.32
2	Thickness (mm.)	1.33
3	Weight (mg.)	20
4	Color	brown
5	Tensile strength (n=3)	15.89 Mpa
	Chemical analysis	
6	Zinc	59.29 mg/kg
7	Copper	15.17 mg/kg
	Biological analysis	
8	NA incubated at 37 ˚C, 24 hrs.	No colony

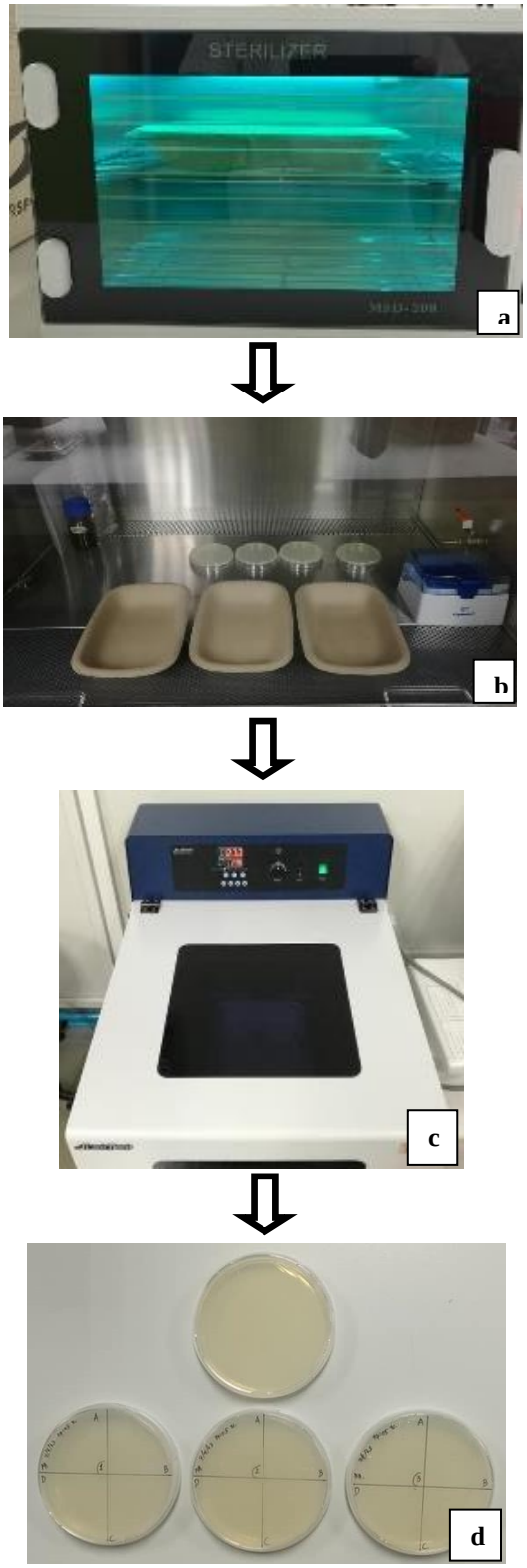

Picture 8: The results of biological analysis (n = 3), a; sample was under UV within 30 min, b; sample were biological analysis, c; sample were incubated at 37 °C, 24 hrs. d; results from biological analysis.

Discussion

Cellulose fibers of rice straw have been identified and used to make biodegradable food containers, biodegradable packaging medical products, and biodegradable industrial packaging products. Technology adaption of rice straw processing seems to have potential to be further commercialized.

From the results presented with physical chemical and biological analysis; this research agreeable with Rushdan Ibrahim et al., 2021 [4]. Table 1: showed tensile strength value of physical analysis was 15.89 Mpa that strength than cellulose fiber from rice straw Juntima et al., 2023 [34] (3.4-5.9 Mpa).

This research was supported by Faculty of Innovative Agriculture and Management, Panyapiwat Institute of Management, and The Rice Department, Ministry of agriculture and cooperatives, Thailand.

Conclusion

This research a new eco-friendly biodegradable packaging from dry rice straw can be add values agriculture wastes, reduce chemical (without sodium hydroxide) on process and more sustainability. From physical chemical and biological analysis, the results as size 12.7x20.32 cm^2, thickness 1.33 mm., weight 20 mg., color was brown, tensile strength (n=3) was 15.89 Mpa. Zinc was 59.29 mg/kg, Copper was 15.17 mg/kg. And without colony on nutrient agar (NA) incubated at 37 ◦C, 24 hrs. Future study will be applying to food and non-food industries and promote to publication using.

References

[1] M. Shahbandeh. (2022). Statista. Agriculture Farming.World production volume of milled rice from 2008/2009 to 2021/2022(in million metric tons) [Online]. Available: https://www.statista.com/statistics/271972/world-husked-rice-production-volume-since-2008/

[2] WorldAgriculturalProduction. (2022). World Rice Production 2020/2021. [Online]. Available: http://www.worldagriculturalproduction.com/

[3] The Bangkok insight. (2021). The potential of biomass fuel to generate electricity from 'Chaff-Rice Straw'. [Online]. Available: https://today.line.me/th/v2/article/DOQ9eo

[4] R. Ibrahim, S.M Sapuan, R.A Ilyas,M.S.N. Atikah.(2021).Utilization of Rice Straw as a Raw Material for Food Packaging. Chapter 12. Bio-based Packaging Material, Environmental and Economic Aspects.

5] S.Somkeawwaan, (2014). Feasibility study of simple production of paper from fresh banana peels and residues from ethanol fermentation. A thesis submitted in partial fulfillment of the requirements for the degree of master of engineering in chemical engineering, Price of Songkran University, Thailand.

[6] W. A. Laftah and W. A. W. A. Rahman. (2021). Rice waste–based polymer composites for Packaging applications: A review. Polymers and Polymer Composites. 29(9S): 621-629.

[7] R. Chollakup, W. Kongtud, U. Sukatta, M. Premchookiat, K. Piriyasatits, H. Nimitkeatkaiand A. Jarerat. (2021). Eco-Friendly Rice Straw Paper Coated with Longan (Dimocarpus longan) Peel Extract as Bio- Based and Antibacterial Packaging. Polymers. 1-13.

[8] S. S. Dhaliwal, V. Sharma, J. Kaur, Arvind K. Shukla, A. Hossain, S. H. Abdel-Hafez, A. Gaber, S. Sayed and V. K. Singh. (2021). Eco-Friendly Rice Straw Paper Coated with Longan (*Dimocarpus longan*) Peel Extract as Bio-Based and Antibacterial Packaging. Sustainability. 14: 29. 1-14. Chemical Engineering rince of Songkla University. 1-129.

[9] FAOSTAT (2020). "Faostat Database," Food and Agricultural Organization Rome, Italy.
[10] A. Satlewal, Agrawal, R., Bhagia, S., Das, P., and Ragauskas, A. J. (2018). Rice straw as a feedstock for biofuels: Availability, recalcitrance, and chemical properties. Biofuels, Bioproducts and Biorefining 12(1), 83-107.
[11] S. Zafar, (2018). "Rice straw as bioenergy resource. BioEnergy Consult. [Online]. Available: Web: https:// www. bioenergyconsult. com/rice-straw-as-bioenergy-resource.
[12] V. Hung, N., Maguyon-Detras, M. C., Migo, M. V., Quilloy, R., Balingbing, C., Chivenge, P., and Gummert, M. (2020). "Rice straw overview: Availability, properties, and management practices," in: Sustainable Rice Straw Management, Springer, ISBN 978-3-030-32372-1. DOI: 10.1007/978-3-030-32373-8.
[13] M. Islam, Praveen Saini, Rahul Das, Shubhra Shekhar, Akhouri Sanjay Kumar, Sinha, and Kamlesh Prasad. (2023). Rice Straw as a Source of Nanocellulose for Sustainable. Bioresources. 18(1), 2351-2385.
[14] P. Lizotte, Savoie, P., and Champlain, A. D. (2015). Ash content and calorific energy of corn stover components in eastern Canada," Energies 8(6), 4827-4838.
[15] M. T. Reza, Emerson, R., Uddin, M. H., Gresham, G., and Coronella, C. J. (2015). Ash reduction of corn stover by mild hydrothermal preprocessing. Biomass Conversion and Biorefinery 5(1), 21-31.
[16] M, Aristizábal, V., García-Velásquez, C. A., and Cardona, C. A. (2016). Integrated production of different types of bioenergy from oil palm through biorefinery concept. Waste and Biomass Valorization 7(4), 737-745.
[17] A. Shariff, Aziz, N. S. M., Ismail, N. I., and Abdullah, N. (2016). Corn cob as a potential feedstock for slow pyrolysis of biomass," Journal of Physical Science 27(2).
[18] X. Yao, Kaili Xu, and Liang, Y. (2016). Comparing the thermo-physical properties of rice husk and rice straw as feedstock for thermochemical conversion and characterization of their waste ashes from combustion," BioResources 11(4), 10549-0564.
[20] E. R. Zanatta, Reinehr, T. O., Awadallak, J. A., Kleinübing, S. J., dos Santos, J. B. O., Bariccatti, R. A., Arroyo, P. A., and Silva, E. A. d. (2016). Kinetic studies of thermal decomposition of sugarcane bagasse and cassava bagasse. Journal of Thermal Analysis and Calorimetry 125(1), 437-445.
[21] A. Mukherjee, Halder, S., Datta, D., Anupam, K., Hazra, B., Mandal, M. K., and Halder, G. (2017). Free radical induced grafting of acrylonitrile on pre-treated rice straw for enhancing its durability and flame retardancy. Journal of Advanced Research 8(1), 73-83.
[22] M. B. Mensah, Jumpah, H., Boadi, N. O., and Awudza, J. A. M. (2021). Assessment of quantities and composition of corn stover in ghana and their conversion into bioethanol. Scientific African. 12.
[23] X. Zhong, Yuan, R., Zhang, B., Wang, B., Chu, Y., and Wang, Z. (2021). Full fractionation of cellulose, hemicellulose, and lignin in pith-leaf containing corn stover by one-step treatment using aqueous formic acid. Industrial Crops and Products 172. artcile no. 113962.
[24] X. Du, Zhang, Z., Liu, W., and Deng, Y. (2017). Nanocellulose-based conductive materials and their emerging applications in energy devices - A review, Nano Energy 35. 299-320.
[25] H. P. S. A. Khalil, Davoudpour Y., Islam, M. N., Mustapha, A. , Sudesh, K.,Dungani, R., and Jawaid, M. (2014). Production and modification of nanofibrillated cellulose using various mechanical processes: A Review. Carbohydrate Polymers 99, 649-665.
[26] J. Gu, and Hsieh, Y.-L. (2017). "Alkaline cellulose nanofibrils from streamlined alkali treated rice straw. ACS Sustainable Chemistry & Engineering 5(2), 1730-37.

[27] A. Sharma, Mandal, T., and Goswami, S. (2017). Cellulose nanofibers from rice straw: Process development for improved delignification and better crystallinity index. Trends in Carbohydrate Research 9(4).

[28] U. Polyium, Boonyaratakalin, T., and Wichiranon, S. (2019). Characterization of physical and mechanical properties of bleaching paper from rice straw. Trans Tech Publications Ltd 891(44776).

[29] D. Kaur, Bhardwaj, N. K., and Lohchab, R. K. (2018). A study on pulping of rice straw and impact of incorporation of chlorine dioxide during bleaching on pulp properties and effluents characteristics. Journal of Cleaner Production 170, 174-182.

[30] M. S. Jahan, Rahman, M. M., Sutradhar, S., and Quaiyyum, M. A. (2015). Fractionation of rice straw for producing dissolving pulp in biorefinery concept. Nordic Pulp & Paper Research Journal 30(4), 562-567.

[31] B. Nasri-Nasrabadi, Behzad, T., and Bagheri, R. (2014). Extraction and characterization of rice straw cellulose nanofibers by an optimized chemomechanical method. Journal of Applied Polymer Science 131(7).

[32] C. Xu, K., Liu, Kang. K., Zheng, Z., Wang, S., Tang, Z., and Yang, W. (2018). Isolation of nanocrystalline cellulose from rice straw and preparation of its biocomposites with chitosan: Physicochemical characterization and evaluation of interfacial compatibility. Composites Science and Technology 154, (8-17).

[33] S. Singh, Dhaliwal, Vivek. Sharma, Vivek. Sharma, Agniva. Mandal, Agniva. Mandal. Authorsgayatri vermagayatri. verma. (2021). Improving soil micronutrient availability under organic farming. Advances in Organic FarmingEdition: 1stChapter: 7Publisher: Woodhead Publishing, Elsevier, Oxford, UK

[34] J. Chungsiriporn, Prukraya Pongyeela and Nirana Chairerk. (2023). Study on the Preparation of Biodegradable Plastic from Rice straw and Chitosan. KKU Sci J. 51(1) 069-007.

基于马尔科夫链 ARIMA 和 YOLOv5 算法的水上巡检系统的设计与应用
DESIGN AND APPLICATION OF AQUATIC INSPECTION SYSYTEM BASED ON MARKOV CHAIN ARIMA AND YOLOv5 ALGORITHM

赖名杰 [1], 张岩 [2], 朱海风 [3], 李奇 [4*]
Mingjie Lai[1], Yan Zhang[2], Haifeng Zhu[3], and Qi Li[4*]

[1,2,3,4] 中国南京工业大学浦江学院计算机与通信工程学院
[1,2,3,4]School of Computer and Communication Engineering,Nanjing Tech University Pujiang Institute, China
[*]**Corresponding Author, E-mail:** 280737222@qq.com

摘要

随着我国工业化和现代化的进程不断加快，为满足河道湖泊渔场的水质检测和水质预测的需求，大幅降低人工定点检测水质和巡视河岸的工作量，本文旨在设计一种基于马尔科夫链 ARIMA 和 YOLOv5 算法作为水质数据预测和巡视检测的水上无人船巡检系统方案 。针对目前常见的水上无人船巡检系统数据处理不佳，视觉识别效果差等问题，本文提出马尔科夫链 ARIMA+YOLOv5 算法的设计方案，首先基于马尔科夫链 ARIMA 深度学习的预测模型解决水质数据处理，并通过运用 YOLOv5 视觉识别算法进行巡视检测。水质传感器采集相关水质数据和摄像头上传视图片，对系统的预测模型和视觉检测模型进行迭代训练，验证。实验测结果表明：水质数据预测结果和图片视觉识别稳定有效，准确率分别到到 60.20% 和 91.66%。

关键词: 马尔科夫链ARIMA YOLOv5 模型预测 目标识别 深度学习

Abstract

With the rapid development of industrialization and modernization, the workload of manual water quality detection and riverbank inspection has been greatly reduced to meet the needs of water quality detection and prediction in rivers and lakes.This paper aims to design a waterborne unmanned boat inspection system based on Markov chain ARIMA and YOLOv5 algorithms as water quality data prediction and patrol detection.Aiming at the problems such as poor data processing and poor visual recognition effect in the current inspection system of unmanned boats on water, this paper proposes a design scheme of Markov chain ARIMA+YOLOv5 algorithm.Firstly, the water quality data was processed based on the Markov chain ARIMA deep learning prediction model, and the YOLOv5 visual recognition algorithm was used for patrol detection. Water quality sensor collects related water quality data and camera uploads visual pictures, and iteratively trains and verifies the prediction model and visual detection model of the system. The experimental results show that the prediction results of water quality data and image visual recognition are stable and effective, with the accuracy of 60.20% and 91.66% respectively.

Keywords: Markov chain ARIMA, YOLOv5, Model prediction, Target recognition, Deep learning

引言

近年来，随着我国经济飞速发展，但是在发展的过程中我们的环境也受到了破坏。2021 年全国污水总排量到高达 750 亿吨，其中有 30%的工业废水和 90%的生活污水未经处理直接排放，导致水体污染严重，水体生态环境遭到严重破坏，除此之外，还有不法分子在禁渔期间进行非法捕鱼，进一步破坏脆弱的河流生态。对于此现象，政府推出河长制进行专人专段河流保护，渔民也要每日定时定点检测水质和巡视。加快推进水上巡检系统建设，对推动环保事业快速进步和渔业高效发展具有重要意义。随着人工智能技术的快速发展，越来越多的学者运用深度学习的方法实现数据预测和图像识别。基于 Mann-Kendall 法和 ARIMA 模型朱颖（2022）实现了武南区域水质预测，基于 ARIMA 与 SVM 唐智 (2018) 实现了湘江流域水质预测，通过 YOLOv5 目标识别算法贺晓倩 (2022) 实现了水面漂浮物的识别，基于深度学习的 YOLOv5 目标识别算法李琦 (2022) 实现了牛群目标检测，基于 YOLOv5 尹凯宸 et al. (2022) 实现了水面垃圾目标检测。

研究目的

上述文献针对水质数据的预测和目标的识别技术还仅限于预测和检测算法本身，并没有对需要处理的海量数据的传输，储存提出一种低功耗、广域网的物联网解决方法，也没有对检测数据和检测目标做出定位；另一方面是目前的系统集成度低，仅能定点对水域进行水质抽样检测，预测或者是水域某一方向进行目标识别检测，因而需要投入大量的时间和精力方可满足巡检一体的功能。

文献综述

针对上述问题，文章在上述研究基础上采用 MC907NBIOT 通信模组实现数据低功耗、广域网的物联网传输方式，同时加入北斗定位模块，将位置数据与检测数据绑定，并应用马尔科夫链 ARIMA 和 YOLOv5 算法，进一步对收集的水质数据进行预测处理和对图像进行识别处理。

研究方法

系统流程与设计思路

本系统采用 STM32F103ZET6 作为硬件水质检测设备主控板，通过 USART 与广和通 MC9074G 模组连接，将检测的水质数据通过 MQTT 通信协议发送 AT 指令上传到 OneNet 云平台。摄像头采用萤石网络摄像头，将检测视频上传到萤石云平台。后端建立 ARIMA 预测模型和 YOLOv5 识别模型，获取云平台上的水质数据和截取图片，存入 MySOL 数据库，在 Windows 系统部署的 ARIMA 预测模型和 YOLOv5 视觉识别算法开始获取原始水质数据和原始图片，并进行水质数据预测和图片检测。前端集成原始水质数据，水质预测走向，图像识别结果，实时定位功能，警报功能和自动巡航功能。前端下发指令经云平台通过 STM32F103ZET6 控制无人船运动，水质传感器投放平台，摄像头舵机转向和毫米波雷达进行自主巡航避障。整体系统架构图如图 1 所视。

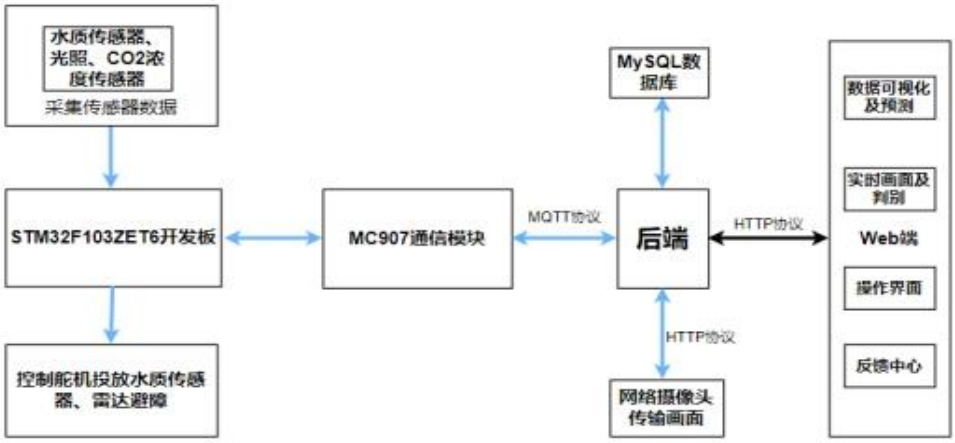

图1: 整体系统架构图

主要硬件设计

1. STM32F103ZET6 开发板

外接5V电源，拥有丰富的外接IO口佘黎煌 et al. (2022)，ADC接口与PH传感器，浊度传感器，TDS传感器，可溶性固体传感器连接，校正后通过ADC转换读取各传感器数值，IIC接口与水温传感器，二氧化碳浓度传感器，光照强度传感器连接，通过IIC协议读取各传感器数值，上述传感器数值形成消息队列稳定发送。

2. MC907 通信模块

由于无人船在户外长时间长距离运行，为使其数据传输达到低功耗广域网的物联网要求，本系统中采用了MC907NB-IOT模组王宇健 (2022)，该模块与STM32进行USART串口通信，接收到来自水质数据传感器检测到的数据，MC907通信模组通过MQTT协议发送指定的AT指令至云端，OneNET云平台接收到相关水质数据。

3. 摄像头模块

在摄像头模块采用萤石网络摄像头CS-BC2，CMOS传感器达到1/2.8英寸，感光效果优异，具有1080P高清分辨率，同时支持夜间红外摄像，满足系统在夜间运行的需求，最高支持15fps的网传帧率，支持H.265视频压缩标准，支持一键AP配网接入萤石物联网云平台，拍摄的实时画面可以通过调用该平台的API可实现画面传输，通过在本地布置的YOLOv5平台进行图像识别。摄像头模块如图2所示。

图 2: 萤石网络摄像头

4. 水质传感器

国家地表水环境质量标准GB3838-2002指出地表水环境质量基本项目有24项。在本系统中，由于是无人船进行的水质检测的特殊工作环境，要求所搭载的传感器做到精简化和轻量化，对国标中的24项基本要求项目不能全部达到。中国生态环境部发布的《环境监测仪器发展指南》提出水质五参数在水质自动监测项目中占有重要地位。五参数包含PH值、水温、电导率、浊度、溶解氧。本系统水质检测传感器模块采用的是HR-6Probe-485-B9六合一水质传感器，检测项目包含PH值、水温、电导率、浊度、盐度、溶解氧。水质传感器如图3所示，传感器参数如表一所示：

图 3: 六合一水质传感器

表 1: 水质传感器参数

搭载传感器	测量范围	精度	分辨率	通信方式
水温传感器	0~50℃	±0.5℃	±0.1℃	
PH 传感器	0~14ph	±0.1ph	±0.01ph	
浊度传感器	0~1000NTU	<3%F.S.	0.1NTU	
电导率传感器	0~5000uS/cm	±1.5%F.S.	1uS/cm	RS-485
溶解氧传感器	0~20mg/L	±0.6mg/L	0.01mg/L	
盐度传感器	0~50%	±0.1%	±0.01%	

ARIMA时间序列预测分析模型

1. 理论基础

ARIMA模型胡衍坤 et al. (2021) 全称为差分自回归移动平均模型（Autoregressive Integrated Moving Average Model），其基本思想是将预测对象随时间推移而形成的数据序列视为一个随机序列，用一定的数学模型来近似描述这个序列。这个模型一旦被识别后就可以用时间序列的过去值及现在值来预测未来值。

ARIMA是多个模型的混合，即AR是自回归，p为自回归项，MA为移动平均，q为移动平均项数，d为时间序列成为平稳时所做的差分次数。在使用ARIMA模型进行预测时，最关键是的确定p、q和d等参数，其主要步骤包括平稳性检验（确定d）、模型识别（确定p和q）、参数估计与诊断检验，最后利用模型进行预测。

由于求和自回归移动平均模型是针对非平稳时间序列所建立的模型，所以可以根据原时间序列是否平稳以及回归中所含(p,q)，以及求和自回归移动平均过程ARIMA(p,d,q)。

对序列进行差分处理后的平稳序列，我们可以使用求和自回归移动平均模型来进行拟合预测，其模型在数学上描述为:

$$\Delta^{d} y_t = \theta_0 + \sum_{i=1}^{p} \phi_i \Delta^{d} y_{t-1} \sum_{j=1}^{q} \theta_j \varepsilon_{t-1}$$

公式中，y_t 为原始时间序列;$\Delta^{d} y_t$ 表示 y_t 经 d 次差分后的平稳序列。ε_t 表示零均值的白噪声随机误差序列。$\phi_i (i = 1,2,\ldots,p)$ 和 $\theta_j (1,2,\ldots,q)$ 为模型的待估计参数，p 和 q 为模型的阶。上述模型记为ARIMA (p,d,q)。

2. 通过马尔科夫过程的ARIMA改进模型建模

马尔可夫链徐梦茹和王学明 (2019)，为状态空间中经过从一个状态到另一个状态的转换的随机过程。该过程要求具备“无记忆”的性质：下一状态的概率分布只能由当前状态决定，在时间序列中它前面的事件均与之无关。这种特定类型的“无记忆性”称作马尔可夫性质。当马尔科夫过程的时间离散且状态离散时，该过程称为马尔科夫链。

根据马尔科夫链将数据序列划分为多个不同状态，分别用$E_1, E_2, E_3, \cdots, E_m$来表示。马尔科夫链从状态$E_i$经过$k$步转移到$E_j$的概率称为转移概率$P_{ij}^{(k)}$为：

$$P_{ij}^{(k)} = \frac{m_{ij}^{(k)}}{M_i}$$

式中，M_i为状态E_i在过程中出现的次数；$m_{ij}^{(k)}$为状态E_i经过k步转移到E_j的次数，得到 1 步状态转移概率矩阵为：

$$P^{(1)} = \begin{bmatrix} P_{11}^{(1)} & \cdots & P_{1m}^{(1)} \\ \vdots & & \vdots \\ P_{m1}^{(1)} & \cdots & P_{mm}^{(1)} \end{bmatrix}$$

根据切普曼－柯尔莫哥洛夫方程，可知k步的状态转移概率矩阵为：

$$P^{(k)} = \left(P^{(1)}\right)^{k}$$

若某状态E_i的初始状态向量为P_0，则经过k步状态转移后的状态向量为：

$$P_k = P_0 \times P^{(k)}$$

3. 建立马尔科夫过程改进ARIMA模型

(1) 建立ＡＲＩＭＡ－ＢＰ神经网络模型。

(2) 用黄金分割法将预测结果序列的误差分为若干个状态区间，并反归一化到原状态区间。

(3) **根据每期**误差落入不同的区间结果计算状态转移概率矩阵，并计算未来多步的状态转移概率矩阵。

(4) 计算未来 n 个时间间隔的状态区间，根据(1)**中的原状**态区间得到区间分界值。

(5) 选择状态分布概率最大的区间，取该区间的均值作为改进的预测值。**整个模型采用**python语言实现，建模流程如图4.

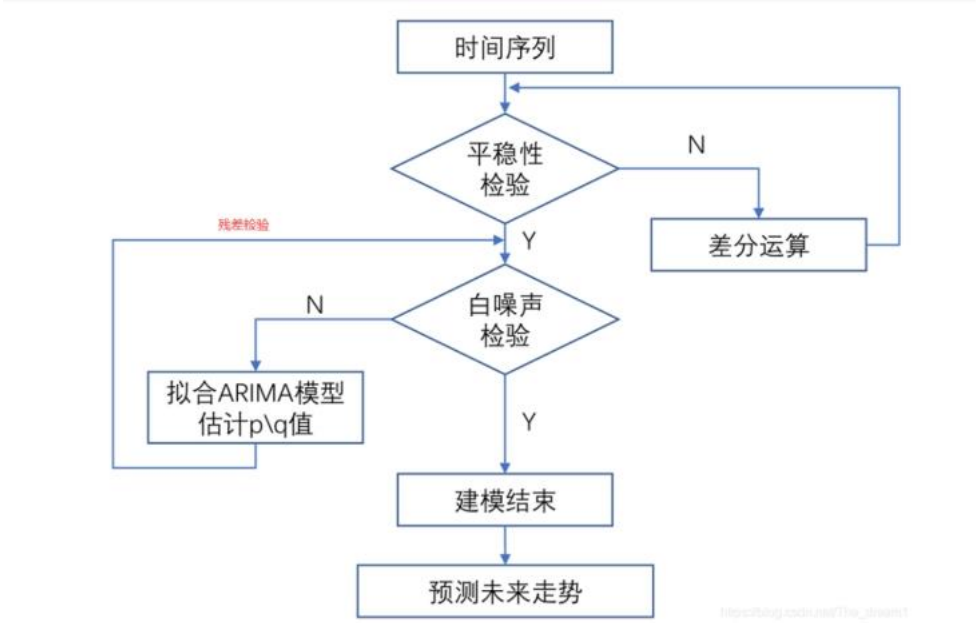

图 4: 马尔科夫链改进ARIMA**模型建模流程**图

4. 制作数据集

本次设计主要以影响水质的温度、日照度、湿度、酸碱度、电导率、二氧化碳含量、透明度、水温、浊度等的因素进行数据加权处理生成时间序列，制作成数据集。

5. 模型预测

利用python语言中的绘图程序，绘制数据的趋势图（图5）

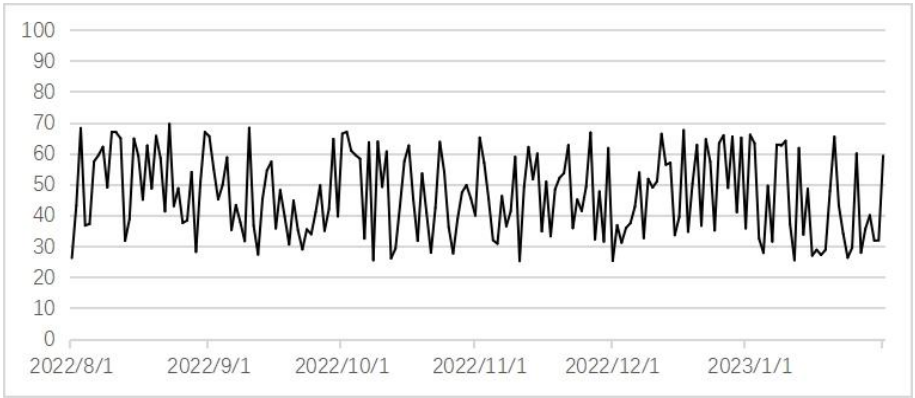

图 5: 数据趋势图

如图5所示数据趋势围绕一个常数上下波动，是一个平稳序列。因此不需要对时间序列进行差分，确定d=0。

6. 数据预测实验结果

将模型预测结果与数据进行拟合，拟合结果如图6所示，实线为真实值，虚线为拟合值。经过多次预测分析，计算得到平均准确率为60.20%。

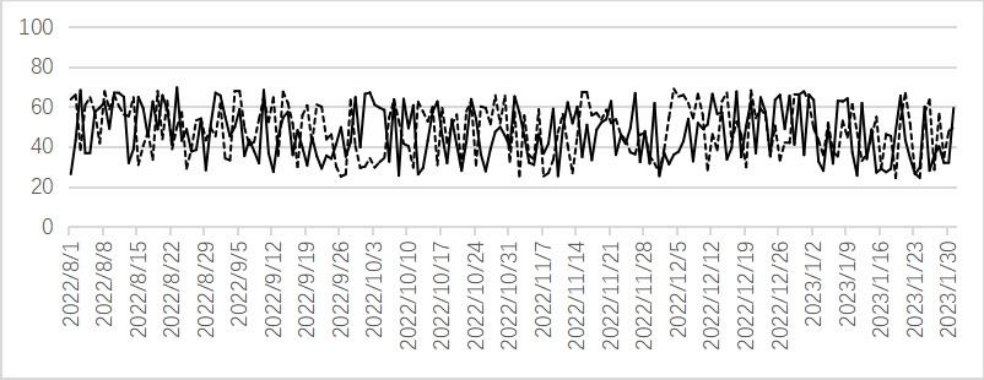

图 6: 真实值与拟合值

7. 数据预测实验结果对比分析

采用某湖泊历史45天PH数据，取前40天作为实验组数据，后5天为对照组数据进行实验。，比较ARIMA模型和马尔科夫链改进的模型预测值，结果如表2所示。

表 2: ARIMA预测值与马尔科夫链改进预测值对比表

真实值 PH	ARIMA 预测值 PH	误差/%	马尔科夫链改进预测值 PH	误差/%
7.31	6.87179487	0.43820513	6.78176283	0.52823717
6.62	6.74358974	-0.12358974	6.63469573	-0.01469573
7.02	7.61538461	-0.59538461	7.35297638	-0.33297638
7.12	7.48717949	-0.36717949	7.09574369	0.02425631
7.06	6.35897436	0.70102564	6.50096874	0.55903126

由表2可以看出，ARIMA模型预测值经马尔科夫链改进后精度有一定的提高。

YOLOv5算法模型

1. 理论基础

YOLOv5 模型李阿娟 (2021) 的网络结构主要由四部分组成： Input、Backbone、Neck、Recision，YOLOv5的网络结构如图5 所示。图7中，Input为图片输入模块，要求输入图像大小为640×640，对于不满足该尺寸的输入图片，可将图片自适应的缩放到 640×640 像素大小。Backbone的作用是对图像进行降采样，减小图片的宽和高，而通道数增加，可提取不同层次的语义信息。YOLO5算法中使用 CSPDarknet53 结构，使用Focus结构作为基准网。Neck位于主干网络和网络头部的中间位置，它以对特征提取的多样性及鲁棒性进行优化。Precision包含分类和回归两个分支，用来完成目标检测结果的输出。

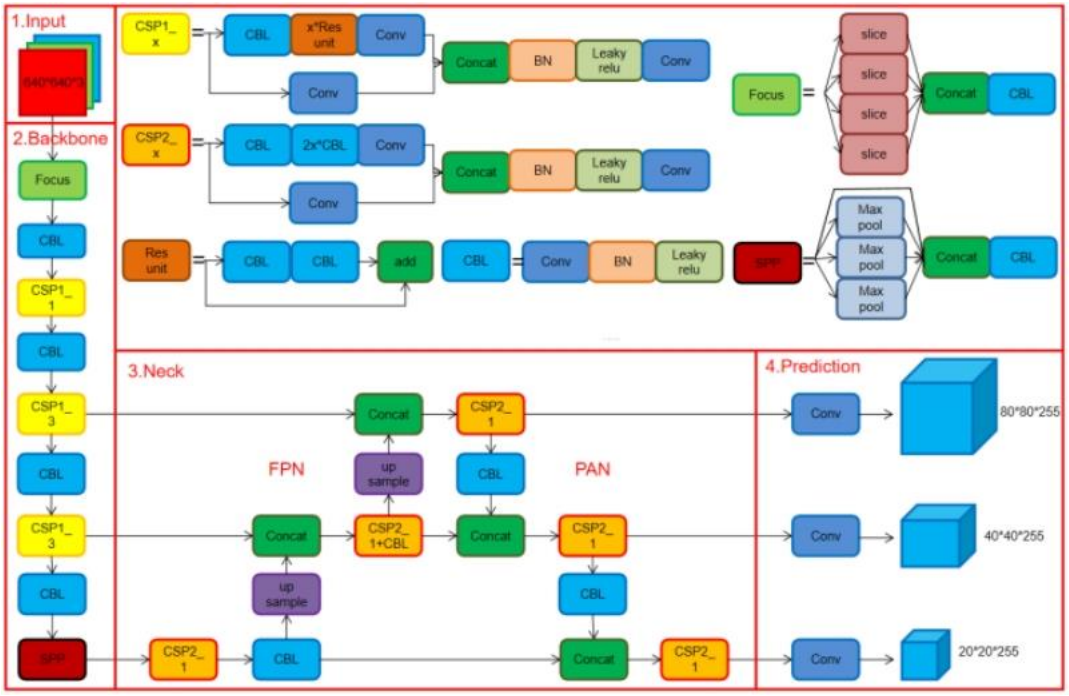

图 7： YOLOv5 模型网络结构

2. 制作数据集

本文基于网络爬虫自建制作了图像数据集，收集了约1000张人体图片进行训练。其中800张用于训练集图像，100张用于验证集图像，100张用于测试集图像。

3. 模型训练

本文训练集的运行环境为WIN10操作系统， cuda10.2、cudnn7.6.5，显卡为NVIDIA TiTANXp，安装pytorch1.7以上版本，用于使用 yolov5 版本 v5.0 代码；设置的训练轮数为100轮。

训练模型的性能指标为精确率、平均准确度、召回率，数学公式如下：

$$precision = \frac{TP}{TP + FP}$$

$$recall = \frac{TP}{TP + FN}$$

$$accuracy = mAP = \frac{TP + TN}{TP + FP + FN + TN}$$

公式中，TP、FP、TN、FN分别表示真阳性、假阳性、真阳性计数和假阳性计数。不同训练轮数的训练结果如图10所示。

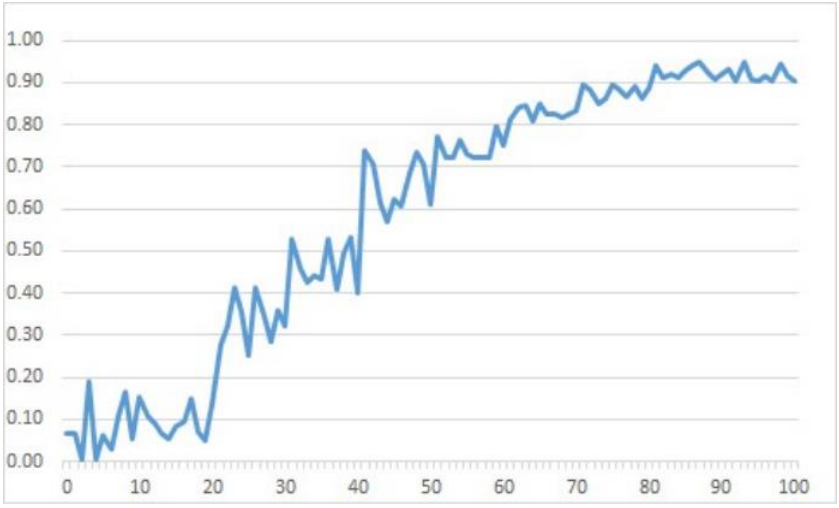

图10：不同阶段训练结果

从中可以看到，在训练轮数较少的情况下，准确率较低，随着训练轮次的不断增加，深度学习算法的训练指标相对更好。

经过100**次的**训练轮次，模型平均准确率达到90%**以上。**

研究结果

本文主要研究了基于马尔科夫链改进的 ARIMA 预测模型在水质数据上的阶段预测和 YOLOv5 算法在巡视过程中对目标物体的识别，实验结果表明本设计的马尔科夫链 ARIMA 模型预测准确率到达了 60.20%，YOLOv5 识别准确率达到了 91.66%。到达设计要求。

讨论

本文设计实现了一种基于物联网的水上巡检系统，可应用于河道湖泊水质检测与预测，政府水务部门的禁渔巡视等。系统主要包括 STM32F103ZET6 主控板、MC907 通信模组、摄像头模块、水质传感器。控制舵机模块投放水质传感器，摄像头拍摄画面，将获取的数据存入 MySOL。其中马尔科夫链 ARIMA 预测模型和 YOLOv5 在 Windows 系统上部署，将两者调试训练完成后，即可从 MySOL 数据库读取数据进行水质数据预测和图像识别。相较于传统系统，本系统功能多元化，适用范围广，同时满足了水质检测预测和水上目标识别。并且系统在满足移动巡检的前提下，预测率和识别率相对较高。

参考文献

王宇健. (2022). NBIOT 技术在工业环境监测中的应用. *现代工业经济和信息化*, (10), 96-97.

尹凯宸, 王欣浦, 吴毅东, 秦民昊, 张金程, & 储昭碧. (2022). 基于 YOLOv5 的水面垃圾目标检测. *电脑知识与技术*, (33), 28-30.

朱颖. (2022). *基于 Mann-Kendall 法和 ARIMA 模型的武南区域水质预测* [硕士论文]. 常州大学. https://kns.cnki.net/kcms2/article/abstract?v=6oglyc8kNW7-eKVf91cuSvEWtnTxxt8IJQdn7zKwHEU46h0nKm8pPwoLjo4A8lVy-Gw7CcVfT26u5qFO1M6Qb-n8o7gSNDtvAVd2Kyvd6KxCmKQasqqaWC7Oqr1g8GC-cnyjTD-PsUE=&uniplatform=NZKPT&language=CHS

李阿娟. (2021). *YOLOv5 算法改进及其现实应用* [硕士论文]. 中北大学. https://kns.cnki.net/kcms2/article/abstract?v=6oglyc8kNW7PQeXsC1yzidArP2U-Exgykz7M94aq01dULno-VBFhIUm-oFct3R3nX78xs6CWilG3eKoVDzDOBbXDMPKJN4-facL0pdGS5Vi0FGKRRuIMHRqkgnpFeU_QB3SDJZotC28=&uniplatform=NZKPT&language=CHS

李琦. (2022). *基于深度学习的牛群目标检测算法及其轻量化研究* [硕士论文]. 杭州电子科技大学. https://kns.cnki.net/kcms2/article/abstract?v=6oglyc8kNW6xU80R_9RPbZhB2cxPxQ2HqOd4nViY1QfGn43ELx_gArOz1W77txNmWufOyPobBvx1a_oUgOusGH7iEmD3DvZu8gMWaj1rS1eyHMzuJFX79v-sGFf2W5ss3Hw0dvlq9JM=&uniplatform=NZKPT&language=CHS

佘黎煌, 刘俊霆, 罗纪青, 刘展鹏, 韩世程, & 刘晨瑞. (2022). 基于 ARM+GPU 的嵌入式系统综合实践案例设计. *计算机教育*, (10), 84-87.

胡衍坤, 王宁, 刘枢, 姜秋俚, & 张楠. (2021). 时间序列模型和 LSTM 模型在水质预测中的应用研究. *小型微型计算机系统*, (08), 1569-1573.

贺晓倩. (2022). *水面漂浮物目标检测算法的研究与设计* [硕士论文]. 西安工业大学. https://kns.cnki.net/kcms2/article/abstract?v=6oglyc8kNW4CRuOKIYs_zcLGr3tbwVYBKsuSsTH9v2teIrFGcZ285S24VT5oyQMNzmJnAeHSk0JCFKlLeu_59lFWcO64_Iw5NrdjF6DqwLuux5XDp_Ky0VZCj3UxqU2xGWxF0WL-VN0=&uniplatform=NZKPT&language=CHS

徐梦茹, & 王学明. (2019). 马尔科夫与 ARIMA 组合模型对地区降雨量的预测研究. *计算机应用与软件*, (03), 34-37+67.

唐智. (2018). *基于 ARIMA 与 SVM 的湘江流域水质预测* [硕士论文] 湖南农业大学. https://kns.cnki.net/kcms2/article/abstract?v=6oglyc8kNW7aWbnxfvv7bqzJGkuw-Lfo5sxNT9_ZP6wT_uTfjkwf8eGOplB_spBr0qdmOioZNEoC1mWqao-FOYT0j9Y-VcI8JLhf1d0JDFerQkyacdlP5A5npFF0wrvKpFEgQN44iQ8=&uniplatform=NZKPT&language=CHS

基于 STM32 及指数平滑算法的矿井智能安全防护装置
INTELLIGENT SAFETY PROTECTION DEVICE FOR MINES BASED ON STM32 MASTER CONTROL AND EXPONENTIAL SMOOTHING ALGORITHM

史建洋 [1], 刘玉飞 [2], 刘舟 [3], 李奇 [4*]
Jianyang Shi[1], Yufei Liu[2], Zhou Liu[3], and Qi Li[4*]

[1,2,3,4] 南京工业大学浦江学院计算机与通信工程学院
[1,2,3,4]School of Computer and Communication Engineering, Nanjing Tech University Pujiang Institute, China
[*]**Corresponding Author, E-mail:** 3563694948@qq.com

摘要

为保障矿井工人工作时的安全，进一步完善矿下安防系统。设计一款基于 STM32 主控，采用多传感器并且运用指数平滑算法进行预测的矿井智能安全防护装置。针对目前矿井下常规的安防措施单一，而且保障工人安全依旧存在一些漏洞等问题，运用多传感器实时监测矿下环境来保障矿工安全，再基于指数平滑算法进行预测，通过对采集的 CO 浓度变化的 2002 条数据进行指数平滑分析进行预测。预测结果与原始数据趋势相吻合，能够作为一个合理的参考模型。

关键词: 物联网 指数平滑预测模型 矿井安全

Abstract

To ensure the safety of mine workers at work and further improve the underground security system. We design an intelligent mine security device based on STM32 main control, using multi-sensors and using exponential smoothing algorithm for prediction. In order to solve the problem that the conventional security measures in the mine are single and there are still some loopholes to ensure the safety of workers, we use multi-sensors to monitor the underground environment in real time to ensure the safety of miners, and then make prediction based on exponential smoothing algorithm by exponential smoothing analysis of the 2002 data collected for the change of CO concentration. The prediction results match with the trend of the original data and can be used as a reasonable reference model.

Keywords: Internet of Things, Exponential Smoothing Prediction Model, Mine safety

引言

中国的矿产资源种类和煤炭资源都位居全球第三，具有丰富矿产资源，矿产资源作为工业的粮食和血液，对中国的发展具有非常重大的战略意义(李丽＆董昕烨,2019)，而作为整体行业正常运作的重中之重莫过于矿下工作人员的人身安全问题，本安全防护装置是针对入矿人员，矿下工作人员所必须佩戴的安全头盔进行科技赋能，提供一款能够与时代接轨的多功能化智能防护头盔。该井矿安防系统主要依托于安防头盔，形成一套完整地上—地下实时通信，实时防控的安防系统。为进一步提高矿井安全提供相应的解决方案，采用多种数据分析、预警、

趋势预测等功能，在物联网下，一体化监测矿井环境，来保障矿工安全，实现系统平台高效运作。

随着大数据应用的不断普及，对于数据处理与分析的能力显得尤为重要，在本套系统中才采用了指数平滑预测模型（李朝晖，1999）（刘洋＆李学文，2020）,结合 STM32 系列主控搭配各类传感器来对矿井工人安全进行保障。在 2022 年，李国伟曾指出当前矿业系统相互之间兼容性差，形成了“信息孤岛”（李国民＆章鳌＆贺耀宜，2022），本设计则加强了整个系统之间的联系，更能体现出数据的价值。而在对于矿工安全这方面也有和我们研究方向不一样的，例如汪东平团队所设计的煤矿井下智能式个体防护装备（汪东平，2021），其主要功能是在高温情况下对工人进行一个安全保障，而本设计则是适用更加普遍的情况，更具有普适性。

目前来说，如今矿井工人的安全防护装置还有较大的提升空间当前矿工所佩戴的绝大部分还是传统安全帽，在 2022 年安徽龙运智能有限公司产出了一种监测矿下甲烷气体浓度的头盔（CN202123246352.X[P]），虽然有功能上的进步但是功能依旧单一。

针对上述问题，文章实现了一套相对智能化的矿井智能安全防护系统，一方面增加了传感器的数量，使得环境数据更加完整，另一方面采用了指数平滑算法对采集到的数据进行模型分析，通过时间序列类方法处理数据，使得矿工在工作时的安全更加有保障。

1、背景介绍

1.1 背景分析

目前来说，如今矿井工人的安全防护装置还有较大的提升空间当前矿工所佩戴的绝大部分还是传统安全帽，仅仅只能提供一些简单的保护功能。在 2022 年安徽龙运智能有限公司产出了一种监测矿下甲烷气体浓度的头盔（CN202123246352.X），虽然有功能上的进步但是功能依旧单一，只能够采集矿井中甲烷气体的浓度，而且拿到该数据之后并没有进行一个数据处理，没能够使得数据价值得到充分发挥。

针对上述问题，文章实现了一套相对智能化的矿井智能安全防护系统，一方面增加了传感器的数量，使得环境数据更加完整，另一方面采用了指数平滑算法对采集到的数据进行模型分析，通过时间序列类方法处理数据，使得矿工在工作时的安全更加有保障。

1.2 优势分析

对于现有市场中的产品来说，本系统可实现的功能更加丰富且完善，本系统除现有产品中可以实现的监测矿下对于甲烷气体浓度的监测、简单照明的功能外，还可以实现对矿井下环境温湿度、可燃气、环境光照强度等信息的采集，除此之外本系统还搭载了激光雷达以便于更便捷的监测矿下环境。而且安徽龙运智能有限公司生产的监测矿下甲烷气体浓度头盔仅仅只是起到一个采集数据的作用并没有对数据进行分析处理，而在如今时代中数据是任何一个产业中尤为重要的生产资料，本团队设计的系统则充分利用了采集的数据，其中运用了指数平滑预测算法，使得整个系统在矿下出现危险情况时能过做到一个预警的作用，大大提高了系统的安全性，能够给矿下工人提供更高的生命保障。除了以上优势之外，本系统还有一大优势，我们将整体数据以及设备信息进行页面化，这样能够推进整个矿井体系的信息化实现，同过客户端可以更加便捷掌握整个矿井的环境、人员、安全信息，大大提高了整个矿井系统的运作效率和安全系数。

2、智能矿井安全防护装置设计

2.1 系统组成

整体的智能安全防护系统主要通过矿产作业人员配戴与本系统实时通信的安全头盔作为实体依托与系统各人员管理平台共同搭建，安全头盔应用绘图（Slam）技术与其他的传感器面向矿下作业的现实场景收集数据信息，通过 LWM2M 通信协议，汇总到 ONENET 云平台，再将数据

通过指数平滑模型进行分析。系统管理平台可主要分为三块：矿下员工工作者，员工管理者，和系统管理者，每一种身份对应不同操作功能，实现闭环管理。.

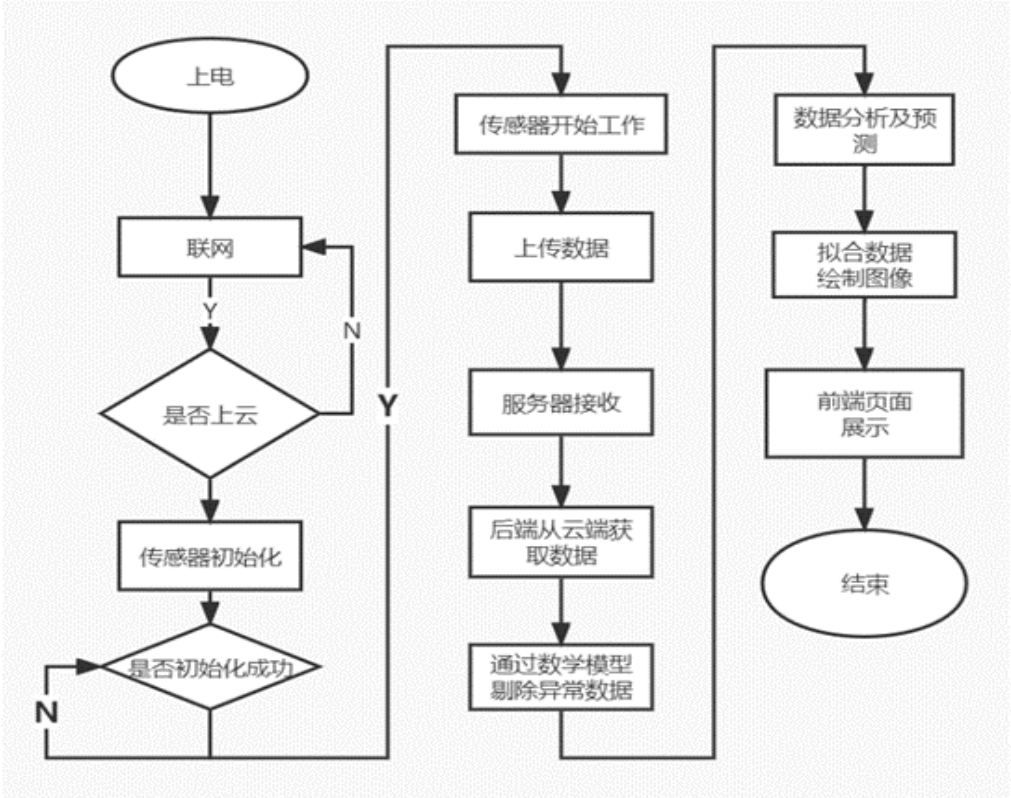

图 1: 系统框架图

2.2 系统设计

2.2.1 系统设计原则

（1）使用尽可能少的重叠功能来分解软件系统，关注点分离系统中的每个模块或服务应专注于一组专用功能。这种方法使理解、开发、维护和增强应用程序变得更加容易。

（2）高凝聚力和松散耦合。内聚性是模块的相关元素属于一起并做一件专门事情的程度。 模块中的所有相关代码应彼此靠近。这有助于减少处理请求的等待时间。使软件组件尽可能松散地耦合，每个模块应尽可能独立于其他模块，以使一个系统中的更改对其他组件的影响最小甚至没有影响。

（3）分布式特征。主要体现在一下几点：具有可扩展性，系统阶段性完成后仍然可以在接下来通过其他的容量的填充来达到需求增长的能力。

2.2.2 系统拓扑结构.

物联网的体系架构主要分为三个层面：感知层，网络层，应用层（申时凯＆佘玉梅，2017）。感知层通过 DHT11 温湿度传感器，MAX30102 心率监测模块，MQ-6 可燃气体检测模块，MQ-7 一氧化碳气体检测，NEO-6M 定位模块，BH1750 光照传感器实现，网络层主要负责对传感器采集的信息进行安全无误的传输，并将收集到的信息传输给应用层。同时，网络层“算”术的应用确保建立实用、适用、可靠和高效的信息化系统和智能化信息共享平台，通信网络是实现“物联网”必不可少的基础设施，实现对各种信息的共享和优化管理。应用层主要解决信息处理和人机界面的问题，也即输入输出控制终端。主要通过数据处理及解决方案来提供人们所需的信息服务（陈

媛，2017）。应用层针对的是直接使用者，为使用者提供丰富的服务及功能，使用者也可以通过终端在应用层定制自己需要的服务：比如查询信息、监视信息、控制信息等等（田翠华，2017）。

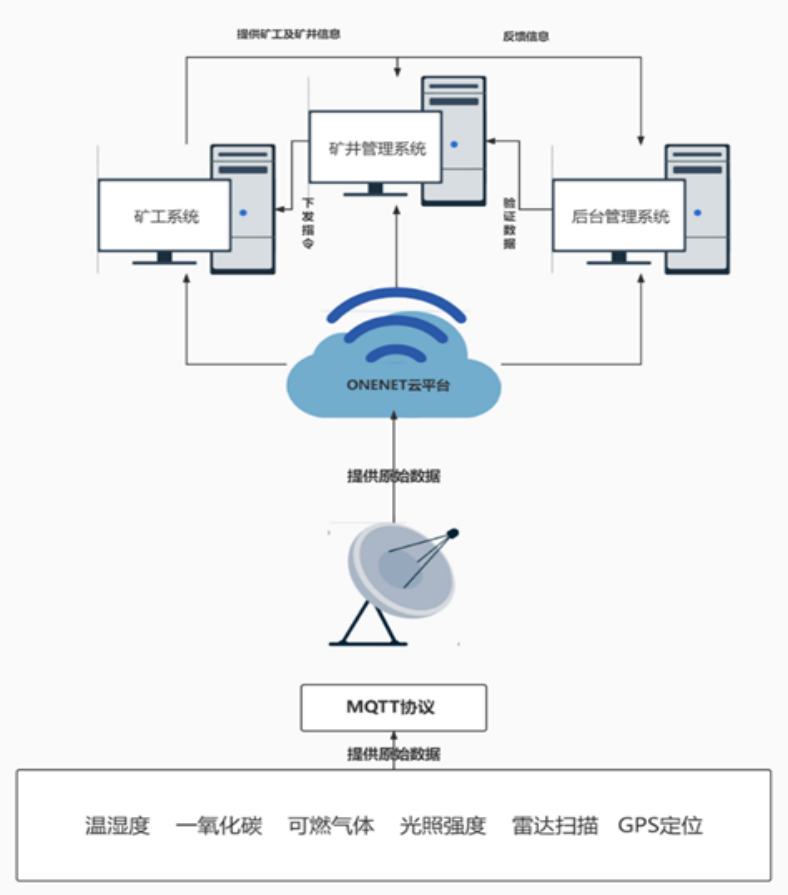

图 2: 系统物联网拓扑图

3、智能矿井安全防护装置系统实现

本系统主要应用于矿下常态化工作作业时期和突发紧急情况的两种场景。针对第一种场景，可将平台分为三部分，对应三种角色，矿下作业的员工，作业员工的管理者与系统技术维护与管理者，分别承担着不同的任务，共同架构起安全防护装置。针对第二种场景，紧急突发状况，这种矿下突发情况一般都为灾难性事件，时间是救援的命脉，在此情形下可通过安全头盔进行临近救援与外来救援相结合，头盔与头盔之间通过蓝牙模块向发送周围工友求救，实现救援及时性。同时通过头盔对于环境参数的检测，预测紧急突发状况的发生。

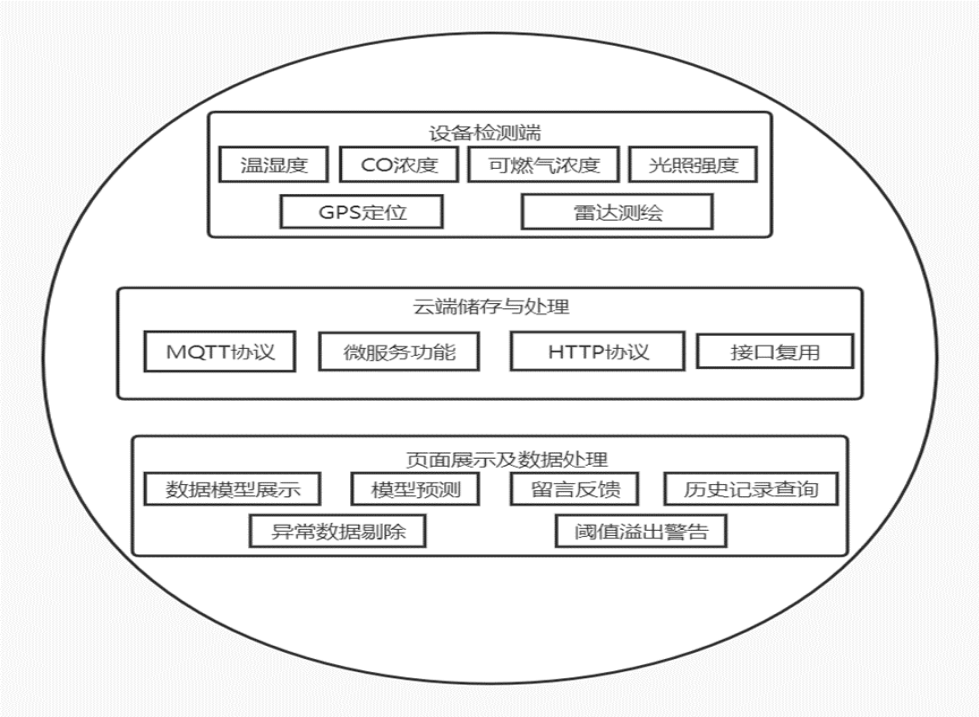

图 3: 系统功能图

3.1 硬件设计

硬件系统设计上主控板采用了 STM32ZET6 和 STM32C8T6；于矿下环境数据采集使用 MQ6(可燃气)MQ7(一氧化碳)DHT11(温湿度)BH1750(光照传感器)NEO-6M(GPS)；过 ZET6 使用广和通的 MC907 通过 LWM2M 协议上传至 Onenet 云平台；光雷达模块单独通过 c8t6 上传数据至 PC 端；PS 定位模块主要用于打卡以及出现危险情形提供坐标的功能；在电源方面我们秉持绿色环保理念使用太阳能板进行充电。

3.1.1 主控板

本设计主控板采用的是 STM32F103ZET6，它拥有的资源包括：64KB.SRAM、512KB FLASH、2 个基本定时器、4 个通用定时器、2 个高级定时器、2 个 DMA 控制器（共 12 个通道）、3 个 SPI、2 个 IIC、5 个串口、1 个 USB、1 个 CAN、3 个 12 位 ADC、1 个 12 位 DAC、1 个 SDIO 接口、1 个 FSMC 接口以及 112 个通用 IO 口。这样一块强大的主板可以支持本设计的所有功能实现。

3.1.2 WIFI模块

本设计采用的 WiFi 模块是广和通 MC907，其是针对中国区域推出的一款高性能、低功耗 LTE Cat NB2 无线通信模组，支持低电压供电，供电范围宽，同时该模块预留了内置 eSIM 卡位置，同时也拥有丰富的外部硬件接口，适合物联网产品的开发。

3.2 接口协议

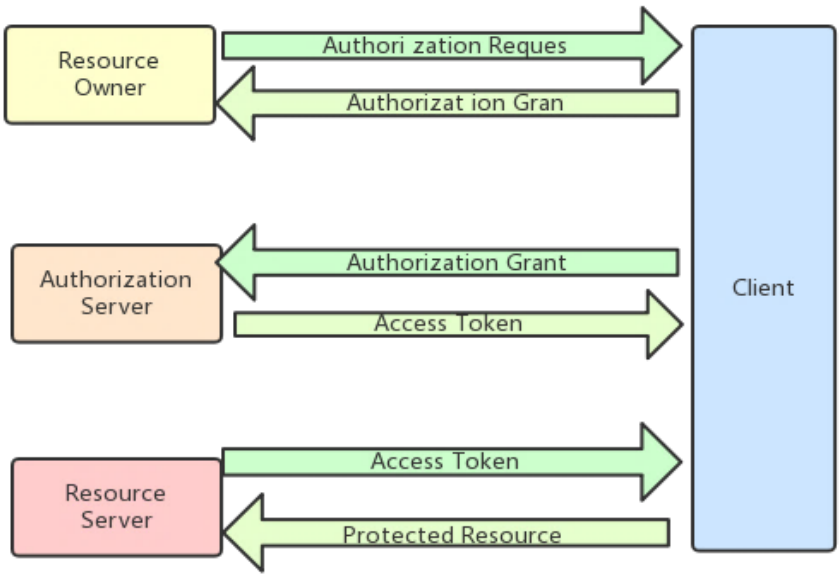

图 4: OAuth2.0 授权流程图

OAuth2.0 是目前最常用的一套安全访问协议，**图 4** OAuth2.0 授权流程图（时子庆＆刘金兰＆谭晓华，2012）。

标准的授权过程主要分为以下六步：

（1）用户打开客户端，客户端向用户请求访问授权。

（2）用户授权客户端。

（3）客户端向认证服务器申请 Token。

（4）认证通过后，发放 Token 令牌给客户端。

（5）客户端携带者 Token，向资源服务器请求资源。

（6）资源服务器验证 Token，通过之后，向客户端开放资源。

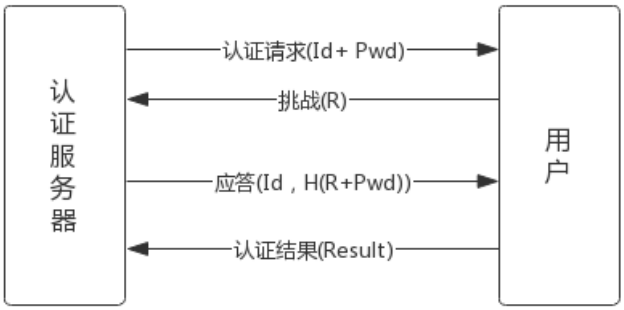

图 5: 基于挑战应答的用户身份认证流程图

本系统在 OAuth2 流程的基础上，使用基于挑战应答的身份认证机制认证用户身份。对每个会话，认证服务器都会给用户客户端发送一个不同的“挑战”字串，用户客户端对此“挑战”做成相应的“应答”，流程如图 5 所示，图中 R 为随机数，HO 为单向 Hash 函数，Id 为用户账号，Pwd 为用户密码。图 5 为基于挑战应答的用户身份认证流程图。

3.3 预测算法

在时间序列中，我们需要基于该时间序列当前已有的数据来预测其在之后的走势，三次指数平滑(Triple/Three Order Exponential Smooth-ing,Holt-Winters)算法可以很好的进行时间序列的预测。针对 CO 和可燃气浓度分别进行了单指数平滑模型，无季节模型，加法模型（王建军＆宋香荣，2016）。

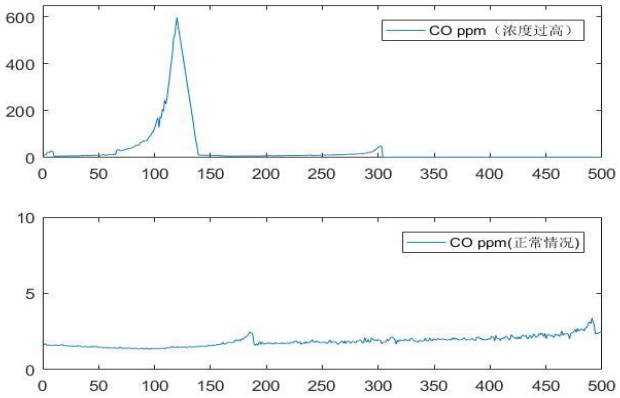

图 6: CO 原始数据图像

在利用指数平滑模型进行分析前，采用图形统计数据做一个大致判断，下面给出指数平滑算法的数据：

一次指数平滑算法基于以下的递推关系（齐颖，2004）：

$$si=\alpha xi+(1-\alpha)si-1$$

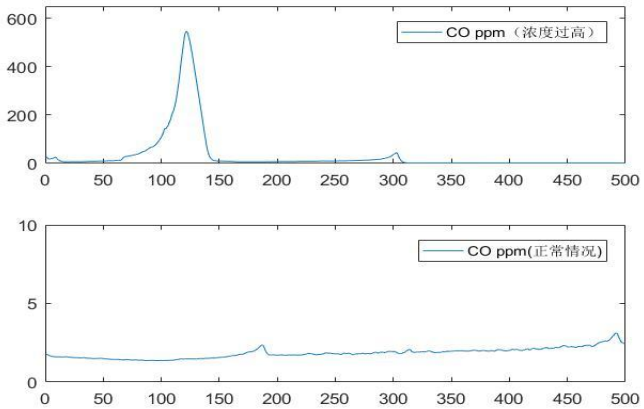

图 7: CO 二次指数平滑预测结果

二次指数平滑保留了趋势的信息，使得预测的时间序列可以包含之前数据的趋势（陈武＆张山江＆侯春华，2016）。二次指数平滑通过添加一个新的变量 t 来表示平滑后的趋势：

$$si=\alpha xi+(1-\alpha)(si-1+ti-1)$$

$$ti=ß(si-si-1)+(1-ß)ti-1$$

三次指数平滑有累加和累乘两种方法，下面是累加的三次指数平滑（云南电网有限责任公司电力科学研究院，2018）。

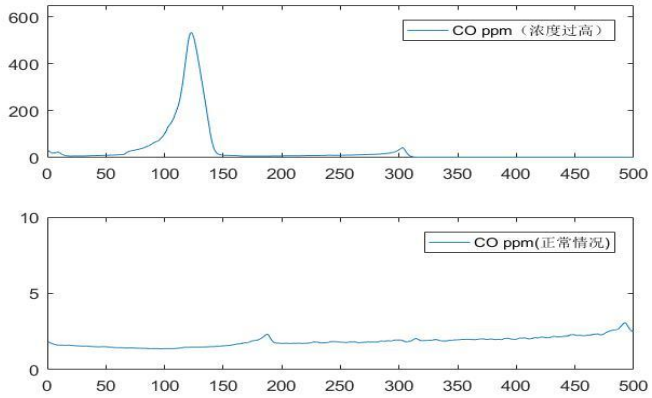

图 8: CO 三次指数平滑预测结果

$$si=\alpha(xi-pi-k)+(1-\alpha)(si-1+ti-1)$$
$$ti=ß(si-si-1)+(1-ß)ti-1$$
$$pi=\gamma(xi-si)+(1-\gamma)pi-k$$ 其中 k 为周期

由数据分析可得，第一次的平滑指数是 0.5；后面两次的平滑指数是 0.7，此时是经过测试最适合的参数。

3.4 Web 端的实现

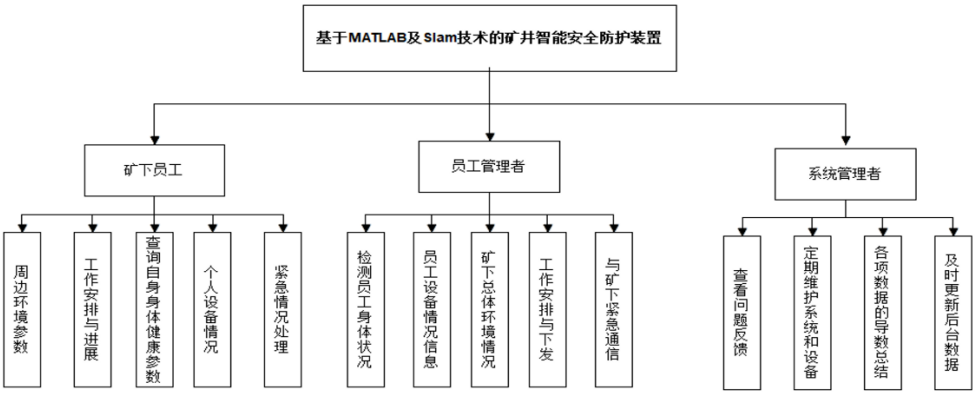

图 9: 系统功能结构图

网页设计上，用户移送设备上发送 SSI 数据，同时用户可以通过浏览器网页和移动端上访问服务器中的页面，服务器由前后端交互和数据库架构，根据用户操作通过 JavaScript 页面逻辑向 springMVC 发送所需请求（张瑞青＆李铁柱，2012），服务器及时给出响应，传达数据给使用界面，SpringBoot 用来处理逻辑和操作数据库（张峰，2017）。

图 10: 设备状态界面界面

矿井智能安全防护装置的基本模块有矿下员工系统、管理人员系统、后台管理人员系统。这三部分子系统还可细分为各子功能模块，具体的系统功能结构。

如图 WEB 服务具有模型预测、数据模型展示、历史数据查询、异常数据剔除、阈值溢出警告（环境出现异常情况）、留言反馈等功能；

4、结束语

文章实现了一套相对智能化的矿井智能安全防护系统，能够对矿下环境情况进行较为全面的监测和环境数据的分析。为解决数据在时间序列中的变化，采用了多次平滑模型，在 MATLAB 中验证了模型的可行性。相较于传统矿工配备的安全措施，文章中系统更加智能化，不仅能够很好反馈矿井下的环境情况，而且更能体现出数据的价值，通过指数平滑预测模型能够较为准确的预测出环境变化的趋势，再尔通过配套 Web 展示实时数据，方便地上了解地下情况，使工作人员以及管理人员更便捷处理相关事务，而且能过让整个矿井更加一体化，提高了整体各方面 的安全性。

研究目的

文章旨在设计一套智能化的矿井安全防护系统，以实现对矿下环境情况进行较为全面的监测和环境数据的分析，从而提高矿井的安全性。

文献综述

近年来，随着物联网技术的发展，越来越多的智能化系统被广泛应用于各个行业。在矿井安全领域，智能化技术的应用也逐渐受到关注。Bhattacharyya et al. （2017）提出了一种基于机器学习的矿井预测系统，能够准确地预测矿井中的异常情况。而 Tong et al. （2020）则提出了一种基于深度学习的矿井安全监测系统，能够对矿井环境进行实时监测和预警。可以看出，在矿井安全领域中，智能化技术的应用已经具有广泛的应用前景。

研究方法

首先，文章采用物联网技术搭建传感器网络，收集并传输环境数据；其次，采用多次平滑模型对时间序列中的变化进行处理，并通过 MATLAB 验证模型的可行性；最后，配合 Web 展示实时数据，方便地上了解地下情况。

研究结果

文章提出的智能矿井安全防护系统相比传统措施更加智能化，能够很好反馈矿井下的环境情况，并通过指数平滑预测模型能够较为准确的预测出环境变化的趋势。同时，配套 Web 展示实时数据，方便地上了解地下情况，使工作人员以及管理人员更便捷处理相关事务，进一步提高了整体各方面的安全性。

讨论

文章提出的智能矿井安全防护系统，采用物联网、数据分析和预测算法技术，能够充分利用环境数据，并通过指数平滑模型进行预测，从而更好地保障矿工们的安全。同时，该系统是一种智能化解决方案，不仅能够实现对矿下环境情况进行较为全面的监测，还能够及时反馈矿井下的环境情况，让工作人员和管理人员更加方便地处理相关事务。

总结与建议

文章成功设计了一套智能化的矿井安全防护系统，并通过数学模型的验证证明了系统的可行性。该系统采用物联网技术搭建传感器网络，能够准确地收集并传输环境数据，并通过指数平滑算法进行预测，方便地展示实时数据，提高整体各方面的安全性。文章的研究成果具有一定的现实意义和推广价值。在系统的实际运用过程中，还需要考虑技术的稳定性和可靠性。在物联网、数据分析和预测算法技术运用中，需要进行不断完善和优化，以确保系统的稳定性和可靠性，并提高系统的精度和效率。同时，还需要注重对用户的培训和使用教育，使得用户能够更好地利用系统，提高矿井的安全性和效益。

参考文献

李丽, 董昕烨(2019). 全球矿业治理的现实困境与中国的未来选择.*国际经济评论*, (5), 123-143.
李朝晖(1999). 指数平滑预测法的运用.*华北科技学院学报*, (2), 41-42, 62
刘洋, & 李学文.(*2020*). 实时数据指数平滑预测分割算法.*数字通信世界*, (3), 93-94.
李国民, & 章鳌 ,& 贺耀宜 ,& 高文 ,& 刘综浏.(2022). 智能矿井多元监控数据集成关键技术研究.*工矿自动化*, (8), 127-130, 146.
汪东平. (*2021*) . 煤矿井下智能式个体防护装备设计.*装备维修技术*, (3), 0145-0145.
申时凯 , & 佘玉梅.(2017). 物联网的技术开发与应用研究. *东北师范大学出版社*
陈媛. (2017) .大数据与社会网络. *上海财经大学出版社*
田翠华. (2017). 基于 GT4 的物联网交通信息服务仿真研究. *厦门大学出版社*
时子庆 ,& 刘金兰 ,& 谭晓华. (2012). 基于 OAuth2.0 的认证授权技术.*计算机系统应用*, (3), 260-264.
王建军 ,& 宋香荣. (2016). 现代应用统计学 大数据分析基础.*机械工业出版社*
齐颖. (2004). 一次指数平滑模型预测法及实际应用.*北京机械工业学院学报*, (4), 50-53,59.

陈武 ,& 张山江 ,& 侯春华.(2016). 二次指数平滑预测模型回归系数计算方法探讨.*统计与决策*, (19), 11-12.

李波.(2018). 电能计量自动化终端自动检测技术.*中国电力出版社*

张瑞青 ,& 李铁柱.(2012). 基于 SpringMVC 的用户登录系统的设计与实现.*科技信息*, (10), 246-247.

张峰.(2017). 应用 SpringBoot 改变 web 应用开发模式.*科技创新与应用*, (23), 193-194.